Early deglacial CO_2 release from the Sub-Antarctic Atlantic and Pacific oceans

Author List: R. Shuttleworth[1], H. C. Bostock[2,3], T. B. Chalk[1], E. Calvo[4], S. L. Jaccard[5,6*], C. Pelejero[4,7], A. Martinez-Garcia[8], G. L. Foster[1]

[1] School of Ocean and Earth Science, University of Southampton, National Oceanography Centre Southampton, Waterfront Campus, European Way, Southampton, SO14 3ZH.

[2] School of Earth and Environmental Science, University of Queensland, Brisbane, Queensland, Australia.

[3] National Institute of Water and Atmosphere, Wellington, New Zealand.

[4] Institut de Ciències del Mar, ICM-CSIC, Barcelona, Catalonia, Spain.

[5] Institute of Geological Sciences and Oeschger Center for Climate Change Research, University of Bern, 3012 Bern, Switzerland.

[6] Institute of Earth Sciences, University of Lausanne, 1015 Lausanne, Switzerland

[7] Institució Catalana de Recerca i Estudis Avançats (ICREA), Barcelona, Catalonia, Spain.

[8] Max-Planck-Institut für Chemie, (Otto-Hahn-Institut), Hahn-Meitner-Weg 1, 55128 Mainz.

*now at Institute of Earth Sciences, University of Lausanne, 1015 Lausanne, Switzerland

Corresponding Author: Rachael Shuttleworth (rs1g16@soton.ac.uk)

Key Words: Deglaciation; Heinrich Stadial 1; CO_2 flux; Boron Isotopes; Southern Ocean; Sub-Antarctic

Highlights:

- Release of deep ocean carbon from the Sub-Antarctic Atlantic and Pacific oceans contributed to the rise in atmospheric CO_2 during the early deglacial (Heinrich Stadial 1; 17.5-15 kyr).
- No evidence for enhanced CO_2 flux from the Sub-Antarctic during the Younger Dryas (12.9-11.5 kyr).
- Large spatial and temporal heterogeneity of CO_2 flux from the Southern Ocean over the last 20 kyr.

Abstract

Over the last deglaciation there were two transient intervals of pronounced atmospheric CO_2 rise; Heinrich Stadial 1 (17.5-15 kyr) and the Younger Dryas (12.9-11.5 kyr). Leading hypotheses accounting for the increased accumulation of CO_2 in the atmosphere at these times invoke deep ocean carbon being released from the Southern Ocean and an associated decline in the global efficiency of the biological carbon pump. Here we present new deglacial surface seawater pH and CO_{2sw} records from the Sub-Antarctic regions of the Atlantic and Pacific oceans using boron isotopes measured on the planktic foraminifera *Globigerina bulloides*. These new data support the hypothesis that upwelling of carbon-rich water in the Sub-Antarctic occurred during Heinrich Stadial 1, and contributed to the initial increase in atmospheric CO_2. The increase in CO_{2sw} is coeval with a decline in biological productivity at both the Sub-Antarctic Atlantic and Pacific sites. However, there is no evidence for a significant outgassing of deep ocean carbon from the Sub-Antarctic during the rest of the deglacial, including the second period of atmospheric CO_2 rise coeval with the Younger Dryas. This suggests that the second rapid increase in atmospheric CO_2 is driven by processes operating elsewhere in the Southern Ocean, or another region.

1. Introduction

The oceans represent the largest carbon reservoir in the atmosphere-biosphere-ocean system, with the Southern Ocean being the primary region for dynamic exchange between the ocean subsurface and the atmosphere. This region therefore exerts a critical control on atmospheric CO_2 levels on various timescales (Sigman et al., 2010). However, the underlying mechanism(s) that drove the rapid CO_2 rise during the most recent deglaciation is still a topic of debate (Galbraith and Skinner, 2020). During the last deglacial, atmospheric CO_2 increased from a stable last glacial maximum value of 190 parts per million (ppm) to pre-industrial levels of 280 ppm. This occurred over two broad, millennial scale, intervals centered around Heinrich-Stadial 1 (HS1, 17.5-15 kyr), and the Younger Dryas (YD, 12.9-11.5 kyr), punctuated by a further centennial increase at 13.8 ka (Bereiter et al., 2015; Fig. 1). This study focusses on the millennial scale episodes of atmospheric CO_2 rise. Several indirect marine proxy records from the Southern Ocean and Antarctic ice cores indicate that the rise in atmospheric CO_2 during both HS1 and the YD may be the result of enhanced upwelling of CO_2-rich subsurface waters in the Antarctic Zone (AZ) (Anderson et al., 2009, Gottschalk et al., 2016, Jaccard et al., 2016, Rae et al., 2018) and/or a decline in biological productivity in the Sub-Antarctic Zone (SAZ) of the Southern Ocean (Lamy et al., 2014, Martínez-García et al., 2014, Jaccard et al., 2016, Thöle et al., 2019).

Recent work, using the carbon isotopic signature of atmospheric CO_2 trapped in Antarctic ice cores ($\delta^{13}C_{atm}$), attempted to distinguish between different sources of carbon during the rapid rises in CO_{2atm} across the last deglaciation ((Schmitt et al., 2012, Bauska et al., 2016); Fig. 1). The initial negative $\delta^{13}C_{atm}$ excursion of -0.3 ‰ during HS1 is proposed to be either the result of enhanced Southern Ocean upwelling of ^{12}C-enriched deep water and/or a decline in the ocean biological carbon pump (Schmitt et al., 2012, Bauska et al., 2016; Fig. 1). The hypothesis of enhanced Southern Ocean overturning during HS1 is supported by a concurrent decline in $\delta^{13}C$ in the surface ocean recorded by planktic foraminifera (Ninnemann and Charles, 1997, Spero and Lea, 2002, Ziegler et al., 2013), an increase in ventilation ages, reducing the radiocarbon depletion of upper circumpolar deep water (Skinner et al., 2010, Burke and Robinson, 2012, Gottschalk et al., 2016), an increase in the deep Southern Ocean water oxygenation (Jaccard et al., 2016, Gottschalk et al., 2016), an increase in opal flux associated with upwelling in the AZ (Anderson et al., 2009; Fig. 1), and an increase in the supply of deep ocean-sourced nitrate to the AZ surface (Studer et al., 2015, Wang et al., 2017). There is also strong evidence for a reduction in the biological carbon pump at HS1 based on productivity and nutrient proxies in Sub-Antarctic Atlantic sediment cores, likely driven by a reduction in the Fe-fertilisation from aeolian dust (Jaccard et al., 2013, Anderson et al., 2014, Martínez-García et al., 2014; Fig. 1). Evidence from the Sub-Antarctic Pacific suggests smaller changes in export production between the Last Glacial Maximum (LGM) and the Holocene (Chase et al., 2003, Bradtmiller et al., 2009, Lamy et al., 2014). The role of this region in deglacial CO_2 rise therefore remains uncertain.

Following HS1, during the Bølling-Allerød/Antarctic Cold Reversal (BA/ACR, 15-13 kyr), atmospheric CO_2 concentrations plateau at 240 ppm, but display a slightly increasing $\delta^{13}C_{atm}$ (Fig. 1), potentially the result of circulation changes in the Southern Ocean and/or regrowth of the terrestrial biosphere (Schmitt et al., 2012, Bauska et al., 2016). This plateau is followed by a second rise in atmospheric CO_2 and a concomitant decrease in $\delta^{13}C_{atm}$ during the YD (12.9-11.5 kyr; Fig. 1). This is proposed to have been driven by a combination of the loss of terrestrial organic carbon, a renewal of upwelling in the Southern Ocean, and rising ocean temperatures (Bauska et al., 2016). Some proxy evidence indicates that circulation-driven changes in the efficiency of the biological carbon pump in the Southern Ocean contributed to this second atmospheric CO_2 increase during the YD (Anderson et al., 2009, Skinner et al., 2014), whilst other datasets show a more muted response (Spero and Lea, 2002, Skinner et al., 2010, Burke and Robinson, 2012, Roberts et al., 2016; Fig. 1).

The modern Southern Ocean acts primarily as a carbon sink (Fig. 2), accounting for approximately 40% of global oceanic uptake of anthropogenic CO_2 (DeVries, 2014). There is however significant spatial variability in this flux, most notably as the result of upwelling of CO_2-rich subsurface water at the Antarctic Polar Front (Takahashi et al., 2012; Fig. 2). Reconstructions of Southern Ocean CO_2 outgassing over the last deglacial would provide important constraints on how the influence of various mechanisms proposed to drive deglacial CO_2 rise evolved (Galbraith and Skinner, 2020). Such reconstructions can be ascertained from planktic foraminifera $\delta^{11}B$ records, however there are currently only a few that directly and quantitatively assess the CO_2 flux in the Southern Ocean over the last deglaciation (Martinez-Boti et al., 2015, Moy et al., 2019). Some of these do not cover the entire 20 kyr period (Martinez-Boti et al., 2015), while those that do are located in the Sub-Tropical Frontal Zone (STFZ) on the edge of the Southern Ocean (Moy et al., 2019). Here we present new boron isotope ($\delta^{11}B$) analyses of planktic foraminifera *Globigerina bulloides* to determine the sea surface CO_2 flux from the Sub-Antarctic Atlantic and Sub-Antarctic Pacific of the Southern Ocean across the entire glacial termination for the first time, and thus further provide additional constraints on the mechanisms of atmospheric CO_2 rise.

2. Methods and Materials

2.1. Samples

The samples used in this study come from two sediment cores covering the last 20 kyr. The first core site (TAN1106-28; 48.372°S, 165.659°E) is located in the northern part of the Solander Trough, south of New Zealand at a water depth of 2798 m. The second core site lies on the southern flank of the Agulhas Ridge in the Sub-Antarctic Atlantic (Piston Core TTN057-6-PC4 (ODP1090); 42°54.5'S, 8°54.0'E) at a water depth of 3702 m. Today, site ODP1090 is situated just north of the Sub-Antarctic Front, the boundary between the AZ and the SAZ, where intermediate waters are formed. Site TAN1106-28 is located on the boundary between SAZ and STFZ, however during the last glacial and deglacial period it is reasoned, based on low productivity and temperatures, that the STFZ shifted northwards within the Solander Trough, thus this core site predominantly records the evolution of Sub-Antarctic surface waters (Bostock et al., 2015). Both sites are located above the modern carbonate lysocline and do not appear to be influenced by dissolution through our study interval (Venz and Hodell, 2002, Bostock et al., 2011).

2.2. Age Model for TAN1106-28 and ODP1090

The age model for TAN1106-28 is based on seven ^{14}C dates of mixed planktic (predominantly *G. bulloides*) foraminifera and three $\delta^{18}O_{G.\ bulloides}$ tie points based on the alignment with the EPICA Dome C δD record using the AICC2012 chronology (Fig. S1). Three of the ^{14}C dates were previously published in Bostock et al. (2015). A core top age of 1000 years with a ±500 year uncertainty was assumed. Following Skinner et al. (2015), reservoir correction ages of 400 yr (<15 kyr) and 1000 yr (>15 kyr) were applied. To assess the influence of reservoir age on the age uncertainty different combinations (0 yr, 400 yr, 1000 yr) were explored, but these showed no significant impact on the age model (Fig. S1). The agreement of the Mg/Ca$_{G.bulloides}$ sea surface temperature with the EPICA Dome C δD record provides good support for this age model, and all age model uncertainty is incorporated into the calculation of ΔpCO_2.

The age model for ODP1090 is based on nine new ^{14}C dates measured on *G. bulloides* (Fig. S2). As in Martinez-Boti et al. (2015) a varying reservoir age of 300 yr (<16 kyr) and 900 yr (>16 kyr) was applied, but constant reservoir ages of 0 yr, 300 yr, and 900 yr were also used to assess the impact that reservoir age uncertainty bears on the age model. Comparison of both the Mg/Ca$_{G.bulloides}$ sea surface temperature to the EPICA Dome C δD record and of the ODP1090 $\delta^{15}N_{G.bulloides}$ of Martínez-García et al. (2014) to the nearby Sub-Antarctic zone coral $\delta^{15}N$ record of Wang et al. (2017), which is independently dated using U-Th and ^{14}C ages provides good support for the robustness of this age model (Fig. S2). As in the TAN1106-28 record, age model uncertainty is propagated into the calculation of ΔpCO_2.

All radiocarbon data were calibrated using SHCal13 (Hogg et al., 2016), and the age models were generated using the ‘UndaTable’ MATLAB software (Lougheed and Obrochta, 2019) which ran 10,000 Monte Carlo simulations using bootstrapping at 30% and a sediment rate uncertainty of 0.1.

2.3. Trace Element and Boron Isotopic Analysis

Twenty-three samples from ODP1090 and fourteen from TAN1106-28, were analysed for Mg/Ca and δ^{11}B at a temporal resolution of 1 kyr and 1.5-2 kyr, respectively. Sediment samples were washed with Milli-Q (>18 MΩcm) over 63 μm sieves and dried in an oven at 50 °C. Sufficient *Globigerina bulloides* individuals from the 180-355 μm (700 individuals), 250-355 μm (500 individuals) or 300-355 μm (300 individuals) size fractions were picked to reach a minimum sample size of ~4 mg of foraminiferal carbonate (equivalent to ~15 ng B). The narrower size fraction range was favoured when possible and was achieved in 75% of samples. Where possible, all size fractions were picked and run as separate samples to investigate the variability between them (Fig. S3). Despite slightly different δ^{11}B values in the measured size fractions, a consistent offset was not evident and most were within analytical uncertainty, thus combining size fractions when required will not affect derived CO_{2sw} interpretations. Samples were prepared and cleaned for trace element and boron isotope analysis following the method described by Henehan et al. (2015). Trace element analysis was performed on a ThermoScientific Element 2 ICP-MS at the University of Southampton using the method described by Henehan et al. (2015). Long-term reproducibility of Mg/Ca and Al/Ca ratio measurements were 4.5% and 25% (2σ) respectively, based on repeat measurements of in-house consistency standards. As Al/Ca is only used to ensure samples had been cleaned sufficiently to remove clay contamination this relatively large uncertainty does not affect the data presented here.

Boron was isolated from the sample matrix via column separation using the ion exchange resin Amberlite IRA-743 (Kiss, 1988). This resin was loaded onto 20 μL Teflon columns, which contained a 3.8 mm diameter polyethylene frit with a pore size of 10-30 μm. These columns were thoroughly cleaned with Teflon distilled 0.5 M HNO_3 and rinsed with 18.2 MΩcm Milli-Q prior to use. The performance of each new column was rigorously tested with a set of reference materials prior to use (NIST SRM 951, JCp-1, and NIST RM 8301f (Stewart et al.)). Since the boron retention of Amberlite IRA-743 is pH dependent, samples were buffered to ≥ pH 5 using a 2M Na-acetate 0.5M acetic acid buffer prior to loading. At pH 5 the resin has a boron partition coefficient of ~10^4 and this allows sufficiently rapid adsorption of boron onto the column for quantitative recovery (Lemarchand et al., 2002). To avoid overloading the columns with ions, the volume of buffer added to the sample was minimised to an upper limit of 600 μl. The buffered samples were then loaded onto the columns in 200 μL aliquots to avoid building up a large hydrostatic head that preliminary data showed was associated with isotopic fractionation due to overly rapid transit time through the column. The matrix was then removed by rinsing with eight separate elutions of 200 μL of Milli-Q, ensuring the walls of the column were well-rinsed. Finally, the sample was eluted by adding 110 μL of 0.5M HNO_3 in five aliquots to ensure all boron was collected. A sixth aliquot was collected separately by loading a final 110 μL of 0.5M HNO_3 and was analysed to confirm boron elution was complete. Isotopic analysis was performed on a ThermoScientific Neptune MC-ICPMS at the University of Southampton following the methods of Foster (2008) and Foster et al. (2013). Reproducibility was calculated based on the relationship between intensity and external reproducibility of repeat analysis of JCp-1 following Rae et al. (2011); typical uncertainty for a 20 ppb sample was 0.20 ‰ at 2σ.

2.4. Carbonate System Calculations

To calculate pH, a species specific calibration needs to be applied to convert measured $\delta^{11}B_{Calcite}$ to $\delta^{11}B_{Borate}$ (Foster and Rae, 2016). *G. bulloides* is symbiont barren so the pH of its microenvironment is lower than that of ambient seawater (Henehan et al., 2016). The $\delta^{11}B_{Calcite}$ - $\delta^{11}B_{Borate}$ calibration used (Raitzsch et al., 2018; Eq. 1) is based on the relationship between plankton tow and core top data (Martínez-Botí et al., 2015, Raitzsch et al., 2018) to $\delta^{11}B_{Borate}$ derived from seasonally resolved carbonate system parameters.

Eq. 1:

$$(\delta^{11}B_{Borate} = \frac{(\delta^{11}B_{Calcite} + 3.58 \pm 11.77)}{1.09 \pm 0.65})$$

These values were used in conjunction with temperature and salinity estimates to calculate pH and CO_{2sw} (Foster and Rae, 2016). Sea surface temperatures (SST) were derived from the measured Mg/Ca on the same samples used for $\delta^{11}B$, using the calibration of Elderfield and Ganssen (2000). Salinity was calculated accounting for the decrease due to ice sheet melt over the deglacial transition as in Palmer and Pearson (2003). A Monte Carlo approach, which randomly selects input parameters within their 2σ uncertainty range was used to produce 10,000 realisations of $\delta^{11}B_{Borate}$, pH and CO_{2sw} to fully propagate uncertainty. These input parameters include (at 2σ) Mg/Ca SST: ±1.8 °C, salinity: ±0.5 psu, and $\delta^{11}B_{Calcite}$: dependent on analysis, but typically ±0.2-0.4 ‰. The $\delta^{11}B$ derived CO_{2sw} record was smoothed by plotting a three point running mean based on a 500 year interpolation of the CO_{2sw} values. The uncertainty is displayed for each data point as the 2.5th, 16th, 84th, and 97.5th percentiles of the Monte Carlo realisations (Fig. 3). Due to the close relationship between change in aqueous CO_2 and change in pH, it is argued that surface ocean pH change is the dominant driver of surface water CO_2 change (Hain et al., 2018). The error associated with defining the second carbonate parameter (alkalinity) in these calculations is therefore not propagated into estimates of CO_{2sw} here (Hain et al., 2018). The above calculations were performed using the 'seacarb' package in R. To determine the role of the Sub-Antarctic Atlantic and Pacific as a source of CO_2 to the atmosphere, ΔpCO_2 was calculated using the contemporaneous CO_{2atm} from the ice core CO_2 record (Bereiter et al., 2015; Eq. 2; Figs. 1, 4):

Eq. 2: $$\Delta pCO_2 = CO_{2sw} - CO_{2atm}$$

When estimating ΔpCO_2, age model uncertainty was propagated using a second Monte Carlo approach. A positive ΔpCO_2 indicates outgassing where the surface ocean around the core site location acted as a source of CO_2 to the atmosphere, whilst a negative ΔpCO_2 indicates the surface ocean was a net sink of CO_2 from the atmosphere. These new boron isotope derived ΔpCO_2 records from the Sub-Antarctic Pacific and Sub-Antarctic Atlantic are then presented alongside a global compilation of published records to explore spatial variability in carbon outgassing from the surface ocean over the deglaciation (Fig. 5). All of these records, and the associated uncertainties, are based on the published pCO_{2sw} data. Error bars vary significantly across these datasets depending on the analytical approach and uncertainty propagation undertaken and reported in each study. In the cases of AA59/1 (Naik et al., 2015) and PC75-2 and PC83-1 (Shao et al., 2019), uncertainty associated with the pCO_{2sw} values were not reported and so a typical uncertainty of ±25 ppm has been applied.

2.5. Carbon Isotopic Analysis

From ODP1090 $\delta^{13}C$ analysis was undertaken every 1 kyr on the planktic foraminifera *G. bulloides*. Twenty individuals from the 300-355 μm size fraction were picked and cracked open individually. Samples were rinsed with methanol, ultrasonicated for 5 seconds, and left at room temperature to dry. Stable isotopic analyses were performed on a Thermo Finnigan MAT253 coupled with a Kiel IV carbonate device at the University of Southampton. A two-point calibration using international standards NBS 18 and NBS 19 was used to correct to Vienna PeeDee Belemnite (VPDB), the standard deviation based on in-house carbonate standard GS-1 is 0.02 ‰ (1σ). Oxygen and carbon stable isotopes on *G. bulloides* were previously published for TAN1106-28 (Maxson et al., 2019).

2.6. Alkenone Analysis

Analysis and characterization of total lipid content for samples from site TAN1106-28 with a temporal resolution of 1-1.5 kyr were performed at Institut de Ciències del Mar in Barcelona following published methods (Villanueva et al., 1997, Calvo et al., 2003, Kornilova and Rosell-Melé, 2003). Briefly, 3-4 g of freeze-dried sediment were loaded into 20 ml Teflon extraction vessels of a MARS6 microwave digestion system (CEM). After addition of internal standards (hexatriacontane and nonadecanol) and subsequent extraction with a dichloromethane/methanol mixture (3:1), the extracts (~ 15 ml) were evaporated to dryness under a gentle nitrogen stream. 6% potassium hydroxide in methanol was used to hydrolyze wax esters and eliminate interferences during quantization of gas chromatographic data. After derivatization with bis(trimethylsilyl)trifluoroacetamide, extracts were dissolved in toluene and then injected in an Agilent 7890 Gas Chromatograph with a flame ionization detector and equipped with a HP-1 capillary column (60 m, 0.25 mm I.D. and 0.25 μm film thickness). H_2 was used as carrier gas. The oven was programmed from 90 °C (holding time of 1 min) to 190 °C at 20 °C/min, then to 290 °C at 6 °C/min with a 40 min hold at 290 °C and finally, from 290 °C to 310 °C at 10 °C/min with a holding time of 6 min. The reproducibility of the analytical methodology was tested with a homogenous sediment standard, which gave analytical errors of 15% in the determination of alkenone concentration.

The vertical flux of alkenones were corrected for redistribution on the ocean floor using U-series analysis of the same sediment samples (Trudgill et al., Submitted) utilising the ^{230}Th-normalisation approach (Francois et al., 2004, Costa et al., 2020; Eq. 3). Here the expected production of ^{230}Th in the water column (β_{230} x z [depth]) is divided by the measured concentration of ^{230}Th, corrected for decay, ($^{230}Th_{xs,0}$). To determine alkenone flux (F_i), the vertical particle flux value was multiplied by the measured alkenone concentrations (c_i).

Eq. 3: $$F_i = \frac{C_i \times \beta_{230} \times z}{^{230}Th_{xs,0}}$$

3. Results

TAN1106-28 records glacial *G. bulloides* boron isotope values of 16.0 ‰, which corresponds to a sea surface pH of 8.25 (Fig. 3). The record from Site ODP1090 exhibits glacial values of 16.5 ‰, which corresponds to a sea surface pH of 8.3. They both present significant negative δ^{11}B excursions around HS1 when TAN1106-28 declines to 15 ‰ (pH 8.15) and site ODP1090 declines to 15.5 ‰ (pH 8.2). At site TAN1106-28, the boron isotope record returns to pre-excursion values (pH 8.25) at 12 ka (Fig. 3), which is comparable to the ODP1090 record, which returns to pre-excursion boron isotopic values (~16.2 ‰) at 15 ka. Both records then hover around 16 ‰, with significant variability of ±0.5 ‰ (pH 8.1-8.25; Fig. 3) until the core top. Both Mg/Ca SST records display an increase of ~5-6 ^{o}C from 19-12 kyr (Fig. 3); Site TAN1106-28 displays glacial SST values of 8 °C, which increase steadily to 14 °C between 19-11 kyr while Site ODP1090 records slightly cooler temperatures of around 7 °C in the glacial, which increase steadily from 19-13 kyr to 12 °C where they stabilise (Fig. 3). Boron isotope derived CO_{2sw} records from TAN1106-28 show glacial CO_{2sw} concentrations around 240 ppm, slightly higher than atmospheric levels from the ice cores, whilst the ODP1090 CO_{2sw} reconstructions are ~200 ppm, similar to the contemporaneous atmospheric CO_2 (Fig. 3). During HS1, from 17-13 kyr, sites TAN1106-28 and ODP1090 show an increase in ΔpCO_{2sw} of up to 100 ppm and 50 ppm, respectively (Fig. 4). From 13 kyr to the end of the deglaciation, reconstructed CO_{2sw} values from site TAN1106-28 and ODP1090 remain similar to atmospheric levels (Fig. 3).

The alkenone concentrations from site TAN1106-28 (this study) and ODP1090 (Martínez-García et al., 2014) declined from 4000-1000 ng/cm^2/kyr and 450 ng/cm^2/kyr to very low values, respectively, immediately prior to the onset of HS1 (17.5-15 kyr), and then remain stable (Fig. 4). At both sites $\delta^{13}C_{\mathit{G.bulloides}}$ show a similar overall pattern of a decline in the early deglacial with a gradual recovery during the Holocene (Fig. 4). However, while the $\delta^{13}C_{\mathit{G.bulloides}}$ from site TAN1106-28 declines throughout HS1, the $\delta^{13}C_{\mathit{G.bulloides}}$ record from site ODP1090 reaches a peak during HS1 and then subsequently decreases.

Comparison of these new ΔpCO_2 records from the Sub-Antarctic Pacific and Sub-Antarctic Atlantic to a global compilation of all existing $\delta^{11}B$ derived ΔpCO_2 records highlights the spatial and temporal heterogeneity of CO_2 outgassing from the surface ocean over the last deglacial (Fig. 5). Whilst each record is influenced by regional processes and is therefore unique to its particular location, they can be compared to provide insights into the mechanisms of CO_2 transfer from the ocean subsurface to the atmosphere during the deglacial, and subsequent atmospheric CO_2 rise, as discussed in the following section.

4. Discussion

4.1. Deglacial Southern Ocean ΔpCO_2

During the last glacial period (>18 kyr) site TAN1106-28 was characterised by surface water CO_{2sw} concentrations of ~240 ppm, making it a source of CO_2 to the atmosphere (Fig. 3, 4). This is interpreted to be the result of frontal migration in this region, during the glacial this site would have been located further in the SAZ, whereas today it is influenced by the highly productive STFZ (Bostock et al., 2015), which would reduce the pre-industrial ΔpCO_2. At ODP1090, there is only one data point from the very late glacial, which suggests this site may have been a minor source of CO_2 to the atmosphere (<20 ppm; Fig. 4). In comparison, the ΔpCO_2 record from core MD97-2106, located south of Tasmania (Moy et al., 2019; Fig. 5), suggests that the Sub-Antarctic was neither a source nor a sink of CO_2 during the glacial. At the start of the deglacial transition (HS1; 18-15 kyr), there was an increase in ΔpCO_2 at both Sub-Antarctic Pacific (TAN1106-28) and Atlantic (ODP1090) sites. These regions of the Southern Ocean became much larger sources of CO_2 to the atmosphere at this time, with ΔpCO_2 values of 100 ppm and 50 ppm, respectively (vs. 20 ppm and -20 ppm today respectively; Fig. 4). These ΔpCO_2 values are similar to changes reported from other regions of the Southern Ocean (Fig. 5) with increases of 50-150 ppm CO_2 evident from Sub-Antarctic Atlantic site PS2498 (Martinez-Boti et al., 2015), and Pacific STFZ sites PC75-2, and PC83-1 (Shao et al., 2019). The current explanation for this shift to carbon source is a reduction in stratification of the deep Southern Ocean (Skinner et al., 2010, Rae et al., 2018) and enhanced upwelling in the AZ (Anderson et al., 2009, Studer et al., 2015). This would have resulted in an enhanced supply of nutrients and light carbon (low $\delta^{13}C$) to the surface waters of the Southern Ocean (Spero and Lea, 2002, Ziegler et al., 2013). This was combined with a decline in biological productivity and efficiency of the carbon pump in the SAZ due to the reduction in dust supply (Lambert et al., 2012, Lamy et al., 2014, Martínez-García et al., 2014, Galbraith and Jaccard, 2015). Comparison to the $\delta^{15}N_{\textit{G. bulloides}}$ record at ODP1090 further supports this assertion as the coeval decrease in $\delta^{15}N$ with ΔpCO_2 (Fig. 1) indicates that a reduction in nutrient utilisation resulted in excess surface water pCO_2 (Martínez-García et al., 2014). This is entirely consistent with the observed decline in alkenone fluxes and planktic $\delta^{13}C$ around 18-12 kyr we observe at TAN1106-28 and ODP1090 (Fig. 4).

In contrast, the waters south of Tasmania (site MD97-2106) remained a minor sink of CO_2 during HS1 (Moy et al., 2019; Fig. 5). The observed discrepancy between sites in the southwest Pacific (MD97-2106 and TAN1106-28; Fig. 5) is interpreted to be the result of the relative location of these two sites with respect to Antarctic upwelling and the scale by which the AZ upwelling signal can be affected by SAZ productivity. For example site TAN1106-28 was located south of the STFZ during the last glacial and deglacial, whilst MD97-2106 remained within the STFZ. Thus, similar to the modern ocean, there was considerable variability in CO_2 flux across the Southern Ocean with the possibility that during the deglacial ΔpCO_2 also decreased northwards from the SAZ towards the STFZ, as it does today (Fig. 2).

The BA/ACR is characterised by an initial rapid increase in atmospheric CO_2 by ~10 ppm over a few hundred years, followed by sustained atmospheric CO_2 levels between 14.7-12.7 kyr (Bereiter et al., 2015). The records from this study show that the CO_2 content of surface waters from the Sub-Antarctic Pacific (TAN1106-28) are still in decline (notwithstanding our relatively low sample resolution), while surface waters from the Sub-Antarctic Atlantic (ODP1090) returned to contemporaneous atmospheric levels during the BA/ACR (Fig. 4). This, accompanied by low alkenone fluxes at both of these sites, indicates that despite low biological productivity, only negligible amounts of CO_2 were being released in the Sub-Antarctic during the BA/ACR (Fig. 4). This perhaps reflects the dominant control AZ upwelling, and the location of the SAZ site relative to this upwelling signal bears on the ΔpCO_2 recorded at the site. The $\delta^{15}N_{G. bulloides}$ record from ODP1090 shows no major change over this period (Fig. 1), which may reflect how AZ upwelling has a greater control on ΔpCO_2, whilst local biological productivity has a more dominant influence on nutrient consumption, and hence on $\delta^{15}N$ (Martínez-García et al., 2014). At TAN1106-28 the planktic $\delta^{13}C$ stabilised following the decline of HS1, whilst at ODP1090 the planktic $\delta^{13}C$ continues to decline, perhaps reflecting low biological productivity during this period (Fig. 4).

These new ΔpCO_2 values are in agreement with the record from site MD97-2106, south of Tasmania (Moy et al., 2019), whilst PS2498 in the Sub-Antarctic Atlantic, west of ODP1090, shows variable flux of ΔpCO_2 of up to 40 ppm throughout this period (Martinez-Boti et al., 2015). Despite this, there is evidence for an overall decrease in ΔpCO_2 of the Sub-Antarctic during the BA/ACR (e.g. surface waters closer to atmospheric equilibrium). This can be explained by a reduction in upwelling of isotopically light carbon and nutrient rich waters in the AZ (Anderson et al., 2009; Fig. 1) and is reflected in the recovery of $\delta^{13}C_{atm}$ (Schmitt et al., 2012, Bauska et al., 2016; Fig. 1).

The onset of the YD is associated with the second major increase (30 ppm) in atmospheric CO_2 and a second decline in $\delta^{13}C_{atm}$ (Schmitt et al., 2012, Bauska et al., 2016; Fig. 1). The boron isotope derived ΔpCO_2 records from the Sub-Antarctic Pacific (TAN1106-28) show that this region was transitioning to a minor sink of CO_2 (although we have limited sample resolution during this interval; Fig. 4). Similarly, the Sub-Antarctic Atlantic (ODP1090) record shows no significant evidence that this region was a major source of CO_2 during this period. The alkenone fluxes from both these locations also remained low throughout the YD (Fig. 4). Although there is a decrease in $\delta^{15}N_{G.bulloides}$ over this period, this is also decoupled from a change in alkenone flux. Consequently Martínez-García et al. (2014) suggest that other influences besides iron fertilisation may affect the $\delta^{15}N_{G.bulloides}$ record during this episode, and so the lack of correlation between the $\delta^{15}N$ and $\delta^{11}B$ derived ΔpCO_2 may not be contradictory. As noted above, the apparent heterogeneity observed in ΔpCO_2 records across the Southern Ocean during the YD also likely reflects that ΔpCO_2 is a combined signal of both AZ upwelling and SAZ productivity and that this variability occurs due to the location of the core site with respect to AZ upwelling. The agreement of the PS2498 ΔpCO_2 record with AZ upwelling (Anderson et al., 2009), but lack of correlation with productivity records from PS2498 itself (Anderson et al., 2014) suggests that this site records a relatively pure AZ signal. Conversely the other Sub-Antarctic Atlantic site ODP1090, which is located further away from Antarctic upwelling, appears to reflect a signal more dominated by the SAZ, especially during the second part of the deglacial. Similarly in the Pacific sector, the lack of any evidence for CO_2 outgassing from site MD97-2416 (Moy et al., 2019) suggests that the sedimentary archive is recording a mixed STFZ and SAZ signal, whilst TAN1106-28 has more of a AZ influence.

Radiocarbon data suggests that the majority of upwelling of deep water carbon had stopped by 15 ka in the Atlantic sector of the Sub-Antarctic (Skinner et al., 2010, Burke and Robinson, 2012; Fig, 1). Furthermore, during the YD, planktic $\delta^{13}C$ values are still low, possibly reflecting a combination of continued low productivity in the region as evidence by low alkenone fluxes, continued upwelling further south in the AZ, and top-down atmospheric forcing (Fig. 4). The lack of evidence for widespread and significant outgassing of carbon from the Sub-Antarctic during the YD suggests that sources of CO_2 outside of the Sub-Antarctic ocean drove the second rise in atmospheric CO_2. Previous studies using $\delta^{13}C_{atm}$, concluded that the CO_2 rise during the YD was primarily associated with a further weakening of the oceanic biological carbon pump due to upwelling in response to an enhancement of the Southern Hemisphere Westerlies alongside oceanic warming (Bauska et al., 2016). The results of this study indicate that the flux of CO_2 from the surface ocean into the atmosphere associated with the enhanced upwelling as evidenced by Anderson et al. (2009) and Studer et al. (2015) must have been limited spatially within the AZ.

4.2. **Deglacial ΔpCO_2: A Global Perspective**

The Sub-Antarctic was not the only location during HS1 where there was significant flux of CO_2 from the surface ocean to the atmosphere. As reviewed by Shao et al. (2019), global records of ΔpCO_2 (Fig. 5) show an enhanced flux of CO_2 from the ocean to the atmosphere during HS1 in the Equatorial Pacific (Palmer and Pearson, 2003, Martinez-Boti et al., 2015), the upwelling regions of the Eastern Equatorial Atlantic (Foster and Sexton, 2014), the North Pacific (Gray et al., 2018), and the North Atlantic (Norwegian Sea) (Ezat et al., 2017). The ΔpCO_2 signature observed in the upwelling regions of the low latitudes is interpreted to be the downstream expression of the Sub-Antarctic surface waters, which are subducted in the SAZ to form intermediate waters (Toggweiler, 1999, Sarmiento et al., 2004, Martinez-Boti et al., 2015). These intermediate depth waters are upwelled in the Eastern Equatorial Pacific, Eastern Equatorial Atlantic, and Indian Ocean (Toggweiler, 1999, Sarmiento et al., 2004). All these low latitude sites also show a decline in planktic $\delta^{13}C$, which has been attributed to either an increase in local upwelling and/or a change in the signature of the source water that is upwelled (Ninnemann and Charles, 1997). Alternatively, this depleted $\delta^{13}C$ signal, which is also evident in the $\delta^{13}C_{atm}$ recorded by ice cores, may have been transferred through the atmosphere (Spero and Lea, 2002). The consistent timing of an increase in ΔpCO_2 with a decline in the $\delta^{13}C$ recorded in ice-cores and planktic foraminifera during the deglaciation observed in this study and in others indicates that an increase in upwelling of $\delta^{13}C$ depleted waters must play an important role.

The increase in ΔpCO_2 from the Norwegian Sea during HS1 (JM-FI-19PC; Ezat et al., 2017) is accompanied by a decrease in planktic $\delta^{13}C$ and an increase in the nutrient concentration proxy Cd/Ca. This is, however, not associated with upwelling of old deep water, as the radiocarbon record at this site indicates younger surface water at this location around 16.5 ka. The enhanced CO_2 concentration at the surface in this case has been interpreted to be the result of either a decrease in biological productivity, rejection of CO_2-rich brine during sea ice formation, the signature of water higher in CO_2 inflowing from the low latitude Atlantic, or a slowdown of deep water formation, leaving carbon to accumulate in the surface waters (Ezat et al., 2017). Conversely, an increased CO_2 flux is absent from sites in the Caribbean Sea and the Western Equatorial Atlantic (ODP999, GeoB-1523; Foster and Sexton, 2014) and far Western Equatorial Pacific (KR05-15; Kubota et al., 2019) during HS1. This observed zonal decrease in ΔpCO_2 gradient is suggested to be the result of intensified and extended upwelling in the east and central Equatorial Atlantic and Pacific, which did not expand as far west as ODP999, GeoB-1532, or KR05-15 (Palmer and Pearson, 2003, Foster and Sexton, 2014, Kubota et al., 2019; Fig. 5).

During the northern hemisphere BA (southern hemisphere ACR) the North Pacific (MD01-2416), Arabian Sea (AA59/21) and Western Equatorial Pacific (ERDC-92) all show evidence of CO_2 outgassing from the surface ocean to the atmosphere (Palmer and Pearson, 2003, Naik et al., 2015, Gray et al., 2018). The North Pacific signal is interpreted to be the result of wind-driven upwelling of CO_2 and nutrient-rich deep water (Galbraith et al., 2007), which continued into the YD (Gray et al., 2018). This is suggested to have led to enhanced export productivity, increased remineralisation of organic carbon at depth, and subsequent widespread hypoxia in the North Pacific Basin (Jaccard and Galbraith, 2012). Although the Arabian Sea records may be due to the enhancement of upwelling in response to an intensification of monsoons during the BA (Naik et al., 2015), its consistency with these other records instead suggest that it was a global feature of the deglacial surface ocean (Fig. 5). Despite evidence of CO_2 outgassing from the surface water, there is no millennial-scale increase in atmospheric CO_2 levels during the BA. It is hypothesised that this outgassing counteracted the return to a stratified Southern Ocean during the ACR (Anderson et al., 2009), which would have increased deep ocean CO_2 storage, allowing atmospheric CO_2 to remain elevated throughout the BA (Gray et al., 2018). The YD is the second major period of atmospheric CO_2 rise over the last deglacial. The only evidence from our global compilation of $\delta^{11}B$ ΔpCO_2 of a greater flux between the oceans and the atmosphere during the YD than in the modern day is from the North Pacific (Gray et al., 2018), Eastern Equatorial Pacific (Martinez-Boti et al., 2015), and North Atlantic (Norwegian Sea) (Ezat et al., 2017; Fig. 5). Both the North Pacific and Eastern Equatorial Pacific sites (Martinez-Boti et al., 2015, Gray et al., 2018) show ΔpCO_2 to be up to 100 ppm during the YD, thus indicating they were major sources of carbon to the atmosphere. The carbon flux in the North Pacific is interpreted to derive from upwelling of carbon-rich water associated with the collapse of North Pacific Intermediate Water formation which resulted in a shoaling of the interior ocean carbon reservoir at the onset of the BA (Gray et al., 2018). In the Eastern Equatorial Pacific, the source of the upwelling and associated CO_2 outgassing is interpreted to be predominantly of Sub-Antarctic origin, with some North Pacific influence, transported via the mode waters (Sarmiento et al., 2004, Martinez-Boti et al., 2015, Toggweiler et al., 2019). Based on the new ΔpCO_2 records presented here, the lack of evidence for significant CO_2 outgassing in the Sub-Antarctic Ocean in the regions of mode water formation during the YD suggests that the CO_{2sw} signal of the Eastern Equatorial Pacific is more heavily influenced by the North Pacific than previously considered. The North Atlantic (Norwegian Sea) may have played a role in the atmospheric CO_2 rise of the YD with site (JM-FI-19PC; Ezat et al., 2017) displaying a minor ΔpCO_2 of up to 20 ppm (Fig. 5). This increase in CO_{2sw} is concurrent with an increase in Cd/Ca ratios measured in the planktic foraminifera, indicative of higher nutrient concentrations at this site suggesting greater upwelling.

In addition to changes in the terrestrial biosphere that occurred during the YD (Köhler et al., 2005), based on our new records from the Sub-Antarctic and a compilation of published ΔpCO_2 records, we propose that enhanced upwelling of carbon-rich deep water in the North Pacific, and Eastern Equatorial Pacific and possibly in the Southern Ocean AZ, played a dominant role in driving the second rise in atmospheric CO_2.

5. **Conclusion**

Core sites TAN1106-28 and ODP1090 show evidence of CO_2 outgassing in the Sub-Antarctic Atlantic and Sub-Antarctic Pacific during HS1. In combination with biological productivity (alkenone concentrations), and upwelling proxies ($\delta^{13}C$) this is interpreted to be due to an increase in Southern Ocean upwelling of old, previously sequestered carbon, and a reduction in primary productivity in response to reduced dust-borne iron (Fe) fertilisation. This outgassing is interpreted to have contributed to the initial rise in atmospheric CO_2 of 35 ppm during HS1 observed in the ice core records, although other sites in the Southern Ocean SAZ and STFZ indicate spatial heterogeneity in the CO_2 flux to the atmosphere during HS1, similar to the Southern Ocean today. A global compilation of similar datasets show that this excess CO_2 in the surface waters of the Southern Ocean was transmitted to the low latitudes via intermediate waters where the excess CO_2 is further outgassed to the atmosphere in the eastern parts of the basins via upwelling.

Conversely, there is no evidence for the Sub-Antarctic acting as a coherent source of CO_2 from the surface ocean during the second episode of atmospheric CO_2 rise in the YD. The only locations that show significant excess CO_2 during this latter half of the deglacial are the North Pacific and Eastern Equatorial Pacific. We therefore suggest that, whilst the Sub-Antarctic played a key role in driving the initial rise in atmospheric CO_2 during HS1, it was not as significant during the second stage of CO_2 rise. However, due to the heterogeneous nature of the Southern Ocean and potential role of the AZ further south, additional records with a greater spatial coverage and higher temporal resolution are required to test this hypothesis.

6. Acknowledgments

We would like to thank the captains, crew and scientists that were involved in collecting the cores used in this study, specifically captain Doug Monks and the crew of the RV Tangaroa who helped collect the TAN1106-28 core. The funding for the TAN1106 voyage was from the Coasts and Oceans Physical Resources program awarded to the National Institute of Water and Atmospheric Research, New Zealand. We thank Bryn Taiapa and Sam Toucanne for providing the additional radiocarbon data for core TAN1106-28, this work was funded by AINSE grant number ALNGRA15502. We also thank Andy Milton, Matt Cooper and Megan Spencer as well as the rest of the Foster lab for laboratory assistance. This project was supported by the Natural Environment Research Council [NE/L002531/1] to R.S. and [NE/J021075/1] to G.L.F., Spanish Ministry of Science and Innovation [CGL2015-68194-R] to E.C. and C.P., S.L.J acknowledges financial support from the Swiss National Science Foundation (SNSF grant PP00P2_172915), and A.M-G acknowledges funding from the Max Planck Society. We also thank the constructive comments of two reviewers.

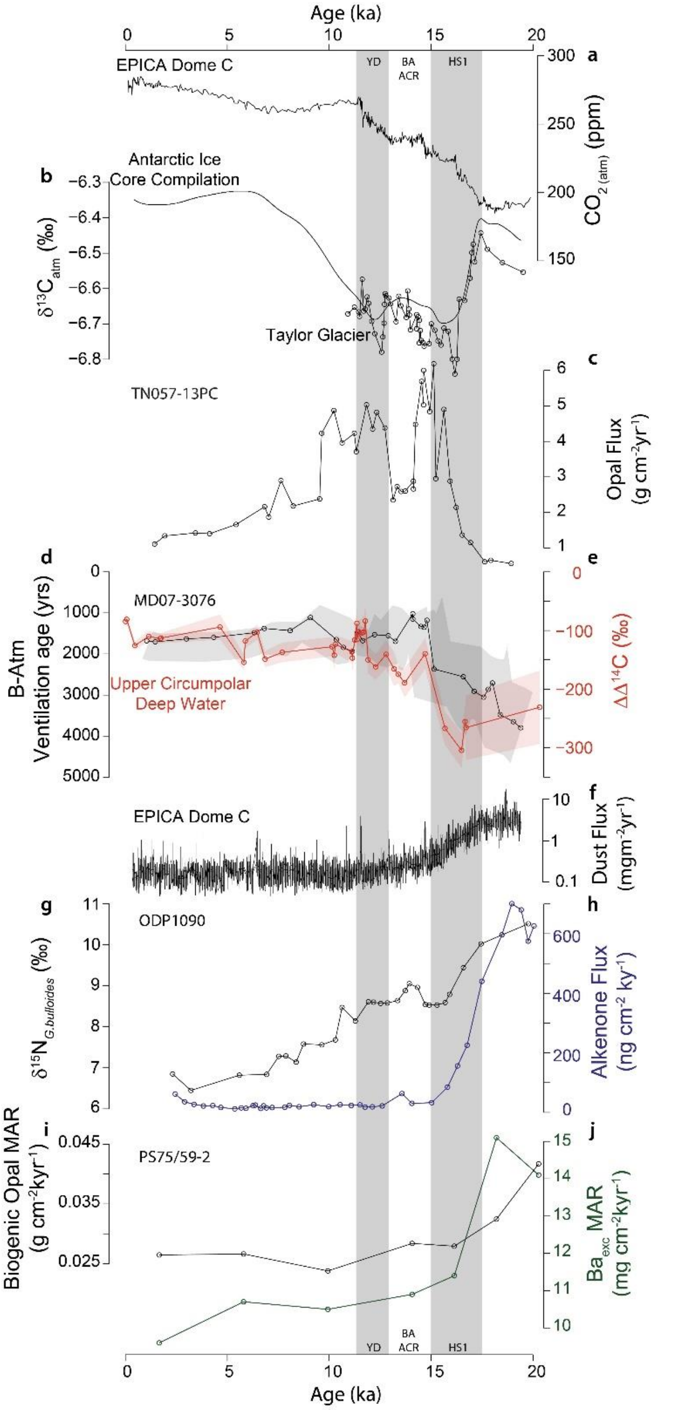

Figure 1. Compilation of marine and ice core proxy records over the last 20 kyr. Two episodes of major atmospheric CO_2 rise (Heinrich Stadial 1 (HS1, 17.5-15 kyr) and Younger Dryas (YD, 12.9-11.5 kyr) are highlighted in grey. **a)** Atmospheric CO_2 reconstructions from ice cores (Bereiter et al., 2015). **b)** atmospheric CO_2 $\delta^{13}C$ (‰) from Schmitt et al. (2012) (line) and Bauska et al. (2016) (points). **c)** Opal Flux (g cm^{-2}yr^{-1}), a proxy for upwelling, from Antarctic site TN057-13PC (Anderson et al., 2009). **d)** Deep-water ventilation from core MD07-3076 (B-Atm) (Skinner et al., 2010). **e)** Offset of deep sea coral $\Delta^{14}C$ from contemporaneous atmospheric levels ($\Delta\Delta^{14}C$ (‰)) (Burke and Robinson, 2012). **f)** EPICA Dome C Dust Flux record (Lambert et al., 2012). **h-g)** $\delta^{15}N_{G.bulloides}$ (‰) and alkenone (ng cm^{-2}kyr^{-1}) flux data from Sub-Antarctic site ODP1090 (Martínez-García et al., 2014). **i-j)** Biogenic Opal Mass Accumulation Rate (MAR) (g cm^{-2}kyr^{-1}) and Ba_{exc} MAR (mg cm^{-2}kyr^{-1}) from Sub-Antarctic site PS75/59-2 (Lamy et al., 2014).

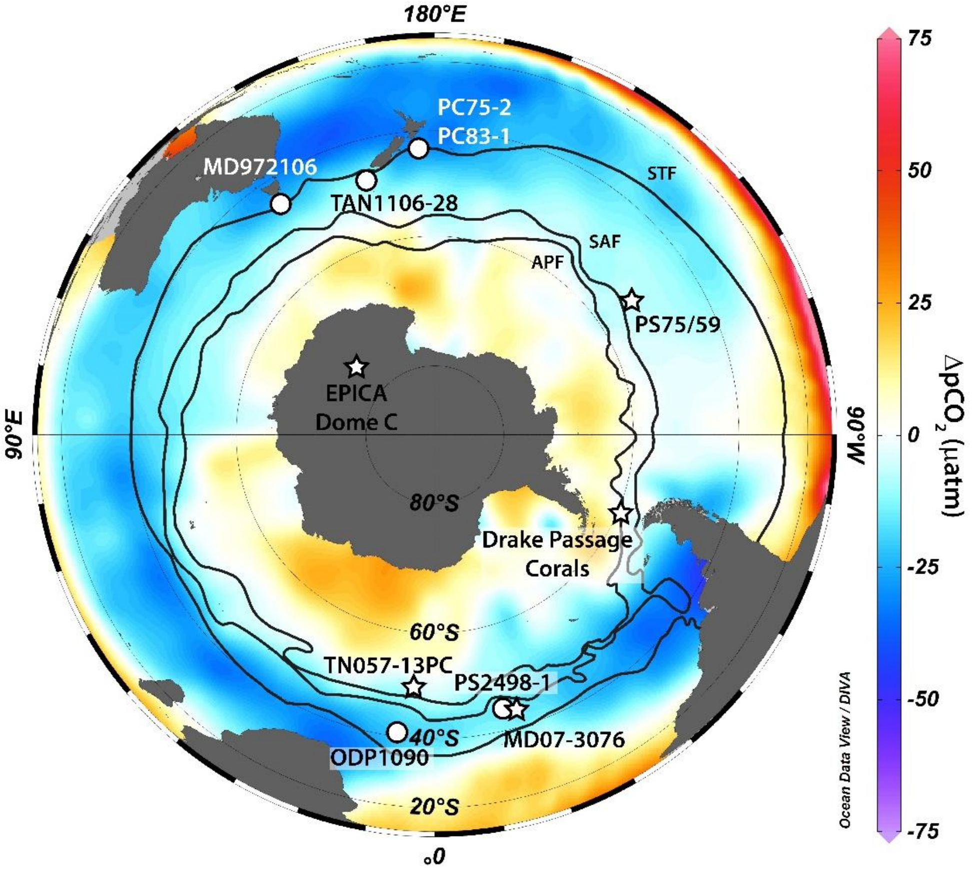

Figure 2. Map of sea surface ΔpCO$_2$ in the modern Southern Ocean. Warm (red) colours show areas where the ocean is a source of CO$_2$ to the atmosphere, cold (blue) colours show sink regions. Circles show core locations for boron isotope records referred to in this study, the sites referenced in Fig. 1 are depicted as stars. Black lines depict the Antarctic Polar Front (APF, Sub-Antarctic (SAF) and Sub-Tropical Frontal Zone (STFZ). Made in Ocean Data View (https://odv.awi.de/) using gridded LDEO pCO$_2$ data of Takahashi et al. (2009) available from (https://odv.awi.de/data/ocean/ldeo-carbon-data/).

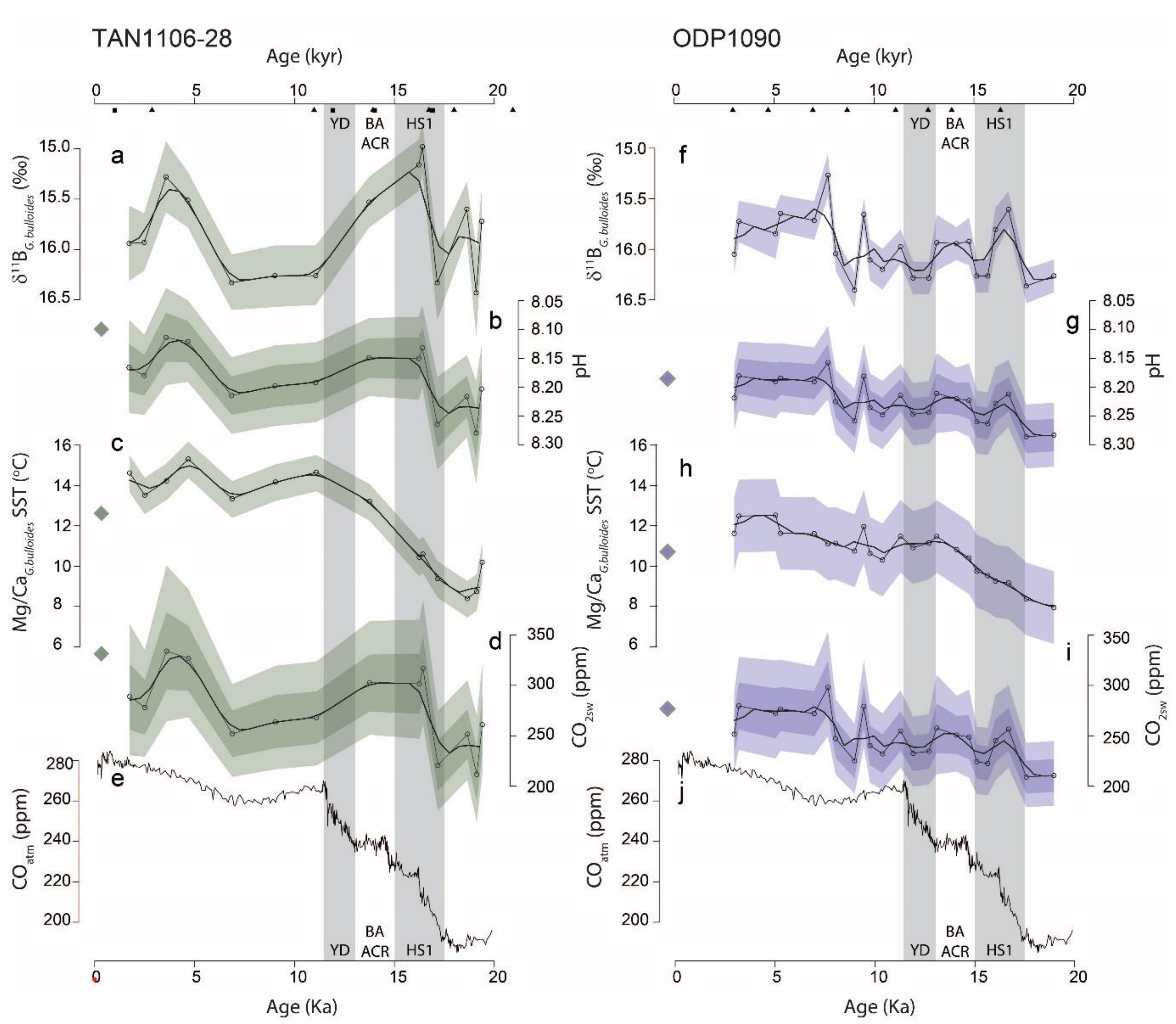

Figure 3. δ^{11}**B, pH, SST and** CO_{2sw} **records from the Sub-Antarctic Pacific (TAN1106-28) and Sub-Antarctic Atlantic (ODP1090) over the last 20 kyr. a-d)** Sub-Antarctic Pacific; **f-j)** Sub-Antarctic Atlantic. Two episodes of major atmospheric CO_2 rise (Heinrich Stadial 1 (HS1, 17.5-15 kyr) and Younger Dryas (YD, 12.9-11.5 kyr) are highlighted in grey. Age model ^{14}C ages are displayed as black triangles, and tie points as black squares. Modern pH, SST and CO_{2sw} values at each site are displayed as diamonds. Bold black line represents the running mean of a 500 year interpolation. **a & f)** $\delta^{11}B_{G. bulloides}$ (‰) with analytical uncertainties (2σ). **b & g)** $\delta^{11}B_{G. bulloides}$ derived pH reconstruction with shaded 68% and 95% uncertainty bands, black line shows calculated equilibrium pH based on atmospheric CO_2. **c & h)** $Mg/Ca_{G. bulloides}$ based sea surface temperature (SST) record with uncertainty margin used within the uncertainty propagation to calculate CO_{2sw}. **d & i)** $\delta^{11}B_{G. bulloides}$ derived CO_{2sw} with shaded 68% and 95% uncertainty bands. **e & j)** Atmospheric CO_2 reconstructions from ice cores (Bereiter et al., 2015).

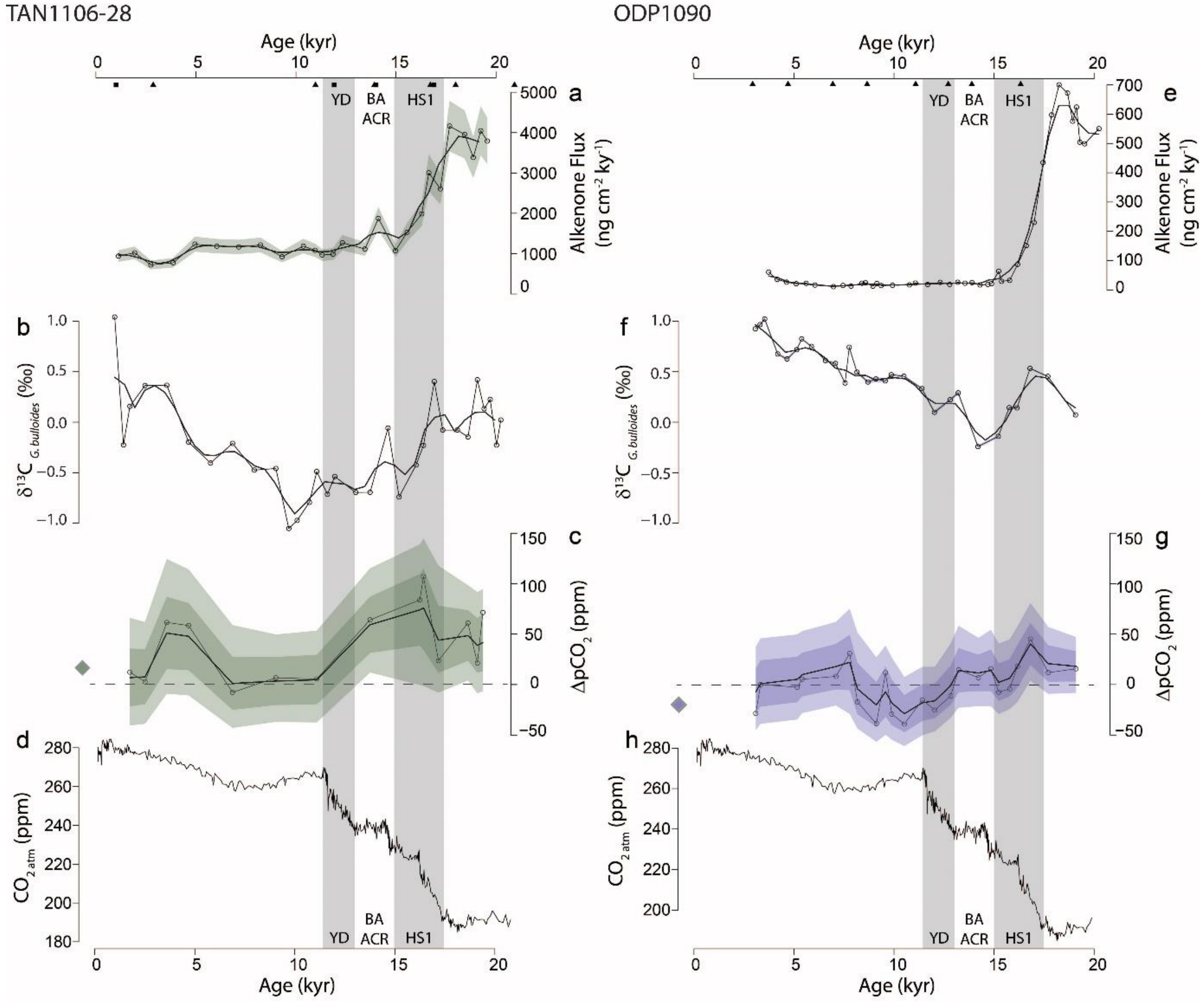

Figure 4. Alkenone flux, $\delta^{13}C_{G.bulloides}$, ΔpCO_{2sw} records from the Sub-Antarctic Pacific (TAN1106-28, a-c) and Sub-Antarctic Atlantic (ODP1090, e-g), and atmospheric CO_2 from ice cores (d & h). Two episodes of major atmospheric CO_2 rise (Heinrich Stadial 1 (HS1, 17.5-15 kyr) and Younger Dryas (YD, 12.9-11.5 kyr) are highlighted in grey. Age model ^{14}C ages are displayed as black triangles, and tie points as black squares. Modern ΔpCO_2 values at each site are displayed as diamonds. Bold black line represents the running mean of a 500 year interpolation. **a)** ^{230}Th normalised alkenone abundance (this study). **b)** TAN1106-28 $\delta^{13}C_{G.bulloides}$ from Maxson et al. (2019). **c)** $\delta^{11}B_{G.bulloides}$ derived ΔpCO_2 with 68% and 95% uncertainty envelopes. **e)** ^{230}Th normalised alkenone flux to site ODP1090 (Martínez-García et al., 2014). **f)** ODP1090 $\delta^{13}C_{G.bulloides}$ (this study) **g)** $\delta^{11}B_{G.bulloides}$ derived ΔpCO_2 with 68% and 95% uncertainty envelopes (this study). **d & h**, Atmospheric CO_2 reconstructions from ice cores (Bereiter et al., 2015).

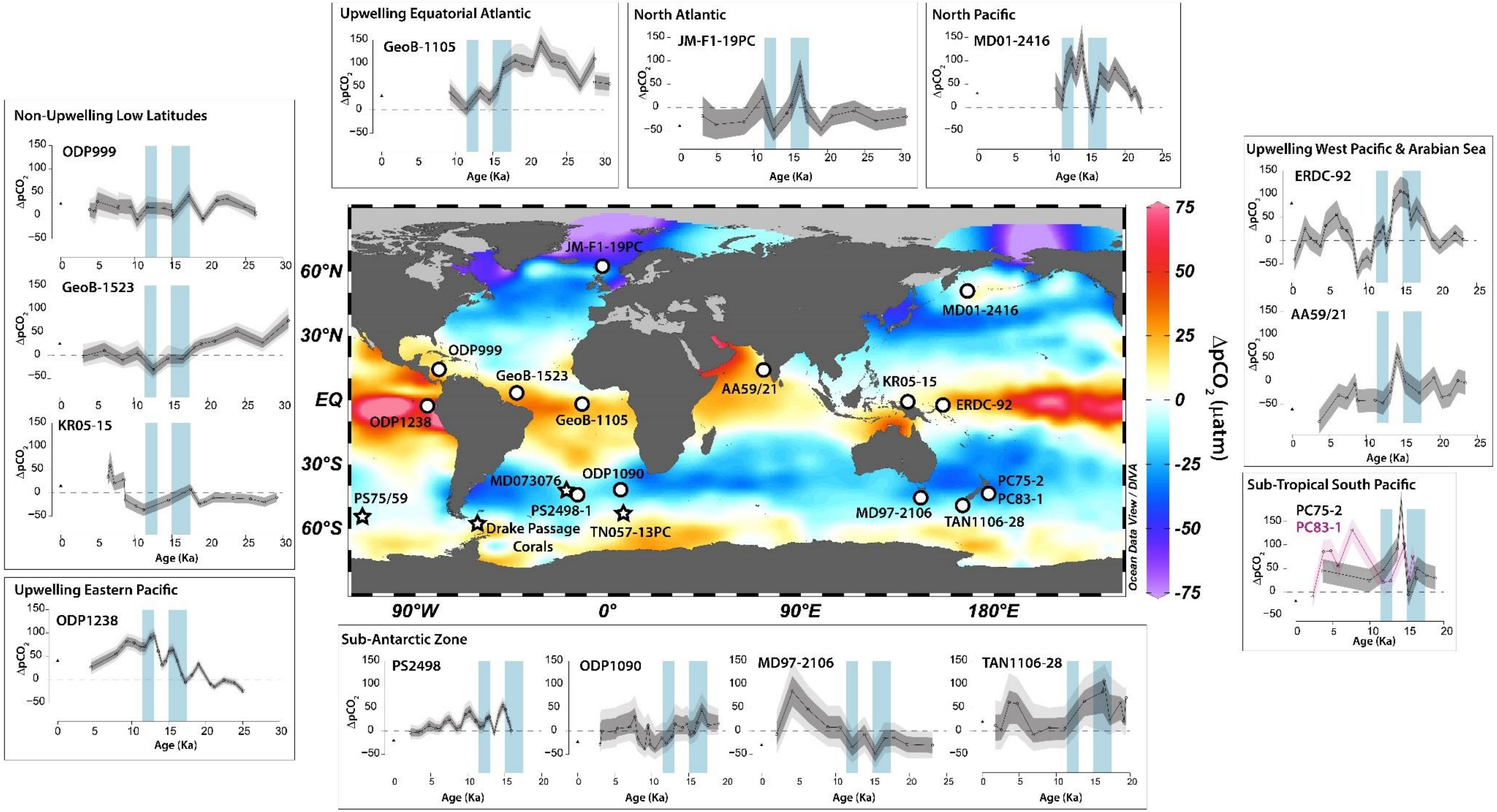
Non-Upwelling Low Latitudes
ODP999
GeoB-1523
KR05-15
Upwelling Eastern Pacific
ODP1238
Upwelling Equatorial Atlantic
GeoB-1105
North Atlantic
JM-F1-19PC
North Pacific
MD01-2416
Upwelling West Pacific & Arabian Sea
ERDC-92
AA59/21
Sub-Tropical South Pacific
PC75-2
PC83-1
Sub-Antarctic Zone
PS2498
ODP1090
MD97-2106
TAN1106-28
ΔpCO2
Age (Ka)
60°N
30°N
EQ
30°S
60°S
90°W
0°
90°E
180°E
PS75/59
MD073076
PS2498-1
TN057-13PC
Drake Passage Corals
Ocean Data View / DIVA
ΔpCO2 (µatm)
75
50
25
0
-25
-50
-75

Figure 5. Map of sea surface ΔpCO_2 in the global modern ocean. Warm (red) colours show areas where the modern ocean is a source of CO_2 to the atmosphere, cold (blue) colours show sink regions. Made in Ocean Data View (https://odv.awi.de/) using the gridded LDEO pCO_2 data of Takahashi et al. (2009) available from (https://odv.awi.de/data/ocean/ldeo-carbon-data/). Datasets taken from Ezat et al. (2017): JM-F1-19PC, Naik et al. (2015): AA59/21, Kubota et al. (2019): KR05-15, Gray et al. (2018): MD01-2416, Palmer and Pearson (2003): ERDC-92, Shao et al. (2019): PC75-2 & PC83-1, this study: TAN1106-28 & ODP1090, Moy et al. (2019): MD97-2106, Martinez-Boti et al. (2015): PS2498 & ODP1238, Foster and Sexton (2014): GeoB-1105, GeoB-1523 & ODP999. In these surrounding plots the two millennial-scale episodes of atmospheric CO_2 rise (Heinrich Stadial 1 (HS1, 17.5-15 kyr) and Younger Dryas (YD, 12.9-11.5 kyr)) are highlighted in blue, black triangles show modern ΔpCO_2 values, errors reflect published values, unless otherwise stated in the manuscript. Core locations depicted as stars are the sites referenced in Fig. 1.

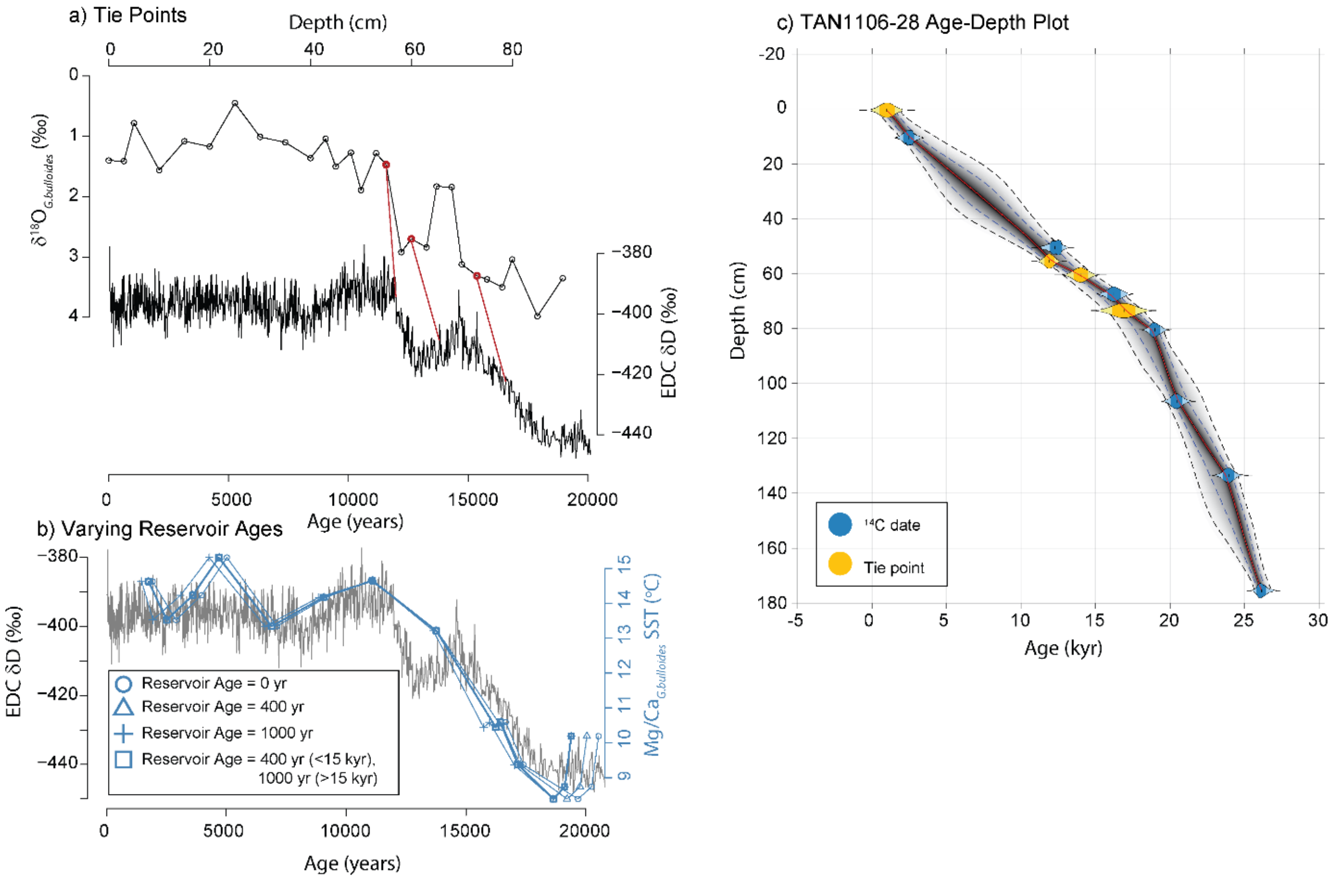

Supplementary Figure 1. Age model for TAN1106-28. a) Shows the $\delta^{18}O_{G.\ bulloides}$ tie points to the AICC2012 δD record. b) Comparison of $Mg/Ca_{G. bulloides}$ derived sea surface temperature (blue) to EPICA Dome C δD Antarctic air temperature record on the AICC2012 age model (grey) (Veres et al., 2013). The variability associated with different reservoir ages is demonstrated by varying shade of blue and symbol (see key). The selected reservoir age is depicted by the bold line with square symbols. c) Age-Depth plot of the age model and the associated age uncertainty.

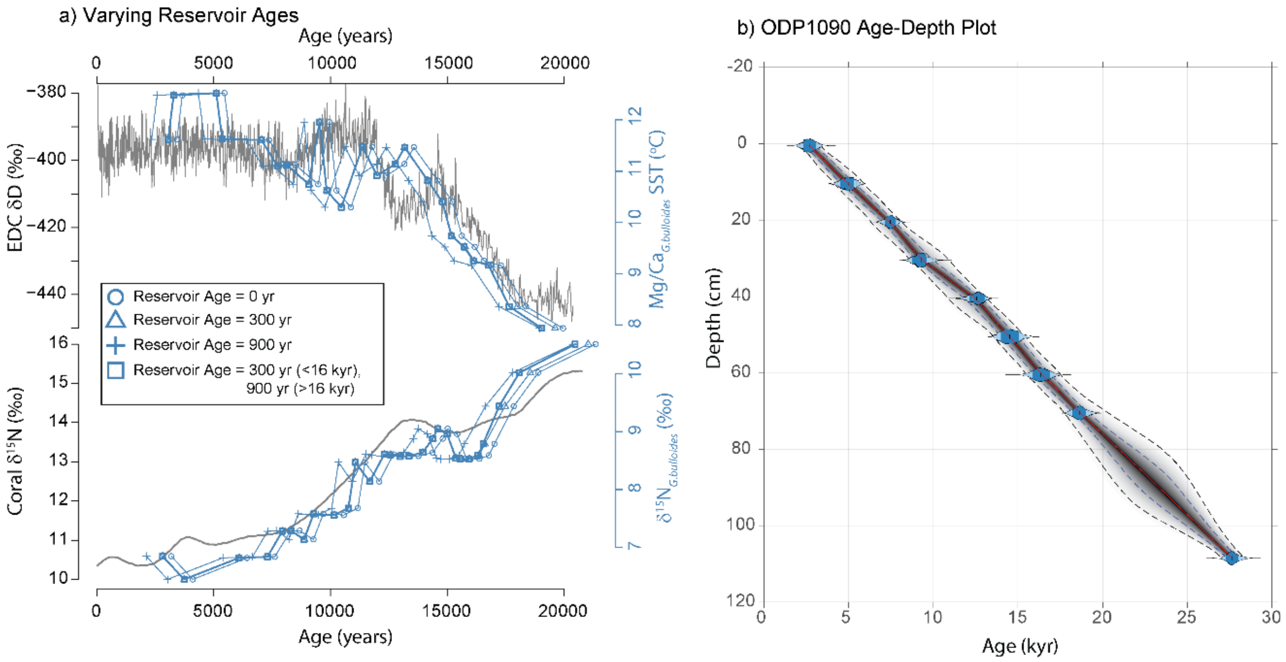

Supplementary Figure 2. Age model for ODP1090. a) Comparison of $\mathrm{Mg/Ca}_{G.bulloides}$ derived sea surface temperature (blue) to EPICA Dome C δD Antarctic air temperature record on the AICC2012 age model (grey) (Veres et al., 2013) and of $\delta^{15}\mathrm{N}_{G.\ bulloides}$ (blue) to nearby coral $\delta^{15}\mathrm{N}$ record of Wang et al. (2017) (grey). The variability associated with different reservoir ages is demonstrated by varying shade of blue and symbol (see key). The selected reservoir age is depicted by the bold line with square symbols. c) Age-Depth plot of the age model and the associated age uncertainty.

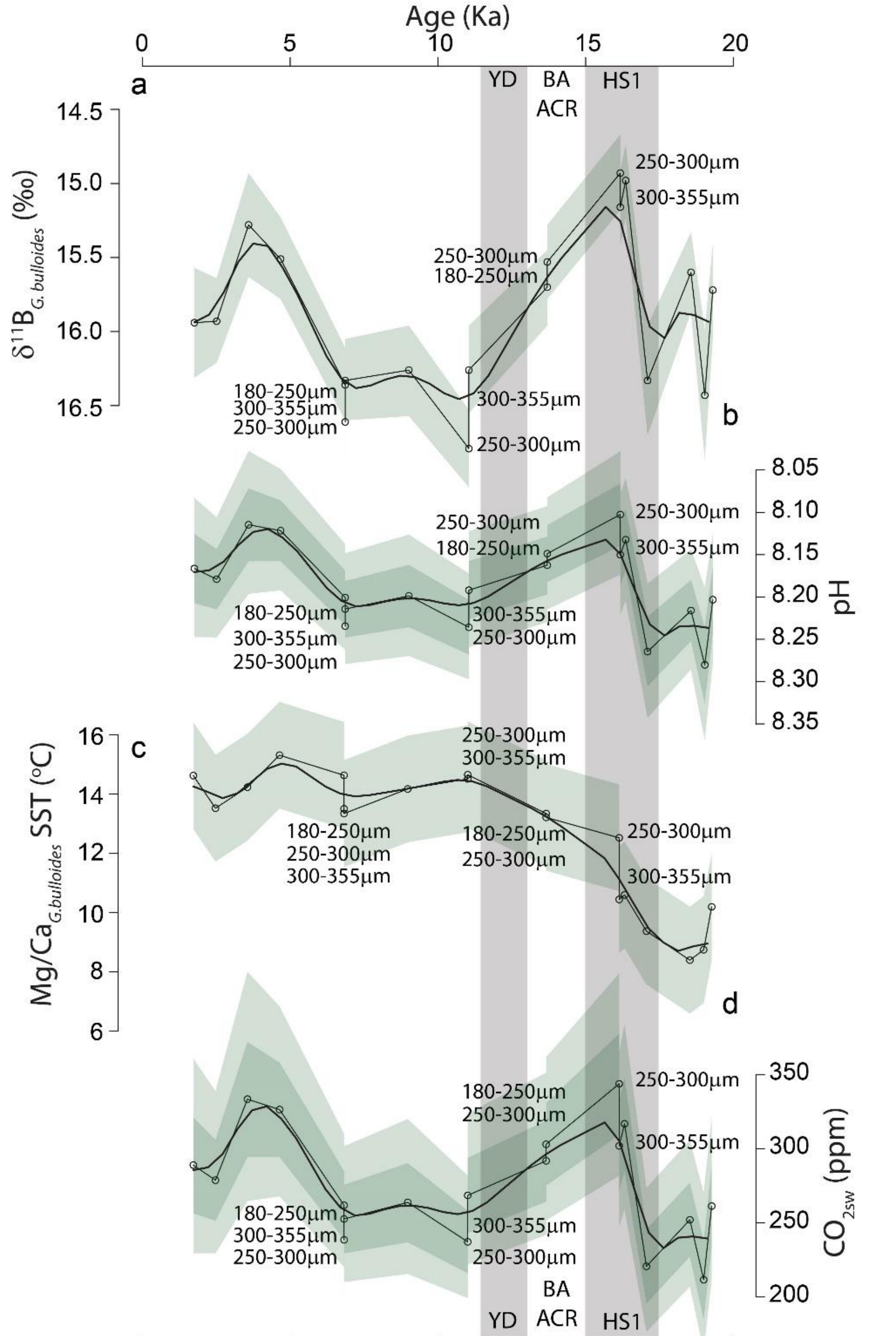

Supplementary Figure 3. Size fraction variability in the δ^{11}B, pH, SST and CO_{2sw} records at site TAN1106-28. Two episodes of major atmospheric CO_2 rise (Heinrich Stadial 1 (HS1, 17.5-15 kyr) and Younger Dryas (YD, 12.9-11.5 kyr) are highlighted in grey. **a)** $\delta^{11}B_{G. bulloides}$ (‰) with analytical uncertainties (2σ, green envelope). **b)** $\delta^{11}B_{G. bulloides}$ derived pH reconstruction with shaded 68% and 95% uncertainty bands. **c)** $Mg/Ca_{G. bulloides}$ based sea surface temperature (SST) record with uncertainty margin used within the uncertainty propagation to calculate CO_{2sw}. **d)** $\delta^{11}B_{G. bulloides}$ derived CO_{2sw} with shaded 68% and 95% uncertainty bands.

7. References

ANDERSON, R. F., ALI, S., BRADTMILLER, L. I., NIELSEN, S. H. H., FLEISHER, M. Q., ANDERSON, B. E. & BURCKLE, L. H. 2009. Wind-Driven Upwelling in the Southern Ocean and the Deglacial Rise in Atmospheric CO2. *Science,* 323, 1443-1448 doi:10.1126/science.1167441.

ANDERSON, R. F., BARKER, S., FLEISHER, M., GERSONDE, R., GOLDSTEIN, S. L., KUHN, G., MORTYN, P. G., PAHNKE, K. & SACHS, J. P. 2014. Biological response to millennial variability of dust and nutrient supply in the Subantarctic South Atlantic Ocean. *Philosophical Transactions of the Royal Society A: Mathematical, Physical and Engineering Sciences,* 372, 20130054 doi:doi:10.1098/rsta.2013.0054.

BAUSKA, T. K., BAGGENSTOS, D., BROOK, E. J., MIX, A. C., MARCOTT, S. A., PETRENKO, V. V., SCHAEFER, H., SEVERINGHAUS, J. P. & LEE, J. E. 2016. Carbon isotopes characterize rapid changes in atmospheric carbon dioxide during the last deglaciation. *Proceedings of the National Academy of Sciences,* 113, 3465-3470 doi:10.1073/pnas.1513868113.

BEREITER, B., EGGLESTON, S., SCHMITT, J., NEHRBASS-AHLES, C., STOCKER, T. F., FISCHER, H., KIPFSTUHL, S. & CHAPPELLAZ, J. 2015. Revision of the EPICA Dome C CO2 record from 800 to 600 kyr before present. *Geophysical Research Letters,* 42, 542-549 doi:10.1002/2014GL061957.

BOSTOCK, H. C., HAYWARD, B. W., NEIL, H. L., CURRIE, K. I. & DUNBAR, G. B. 2011. Deep-water carbonate concentrations in the southwest Pacific. *Deep Sea Research Part I: Oceanographic Research Papers,* 58, 72-85 doi:https://doi.org/10.1016/j.dsr.2010.11.010.

BOSTOCK, H. C., HAYWARD, B. W., NEIL, H. L., SABAA, A. T. & SCOTT, G. H. 2015. Changes in the position of the Subtropical Front south of New Zealand since the last glacial period. *Paleoceanography,* 30, 824-844 doi:10.1002/2014PA002652.

BRADTMILLER, L. I., ANDERSON, R. F., FLEISHER, M. Q. & BURCKLE, L. H. 2009. Comparing glacial and Holocene opal fluxes in the Pacific sector of the Southern Ocean. *Paleoceanography,* 24.

BURKE, A. & ROBINSON, L. F. 2012. The Southern Ocean's Role in Carbon Exchange During the Last Deglaciation. *Science,* 335, 557-561 doi:10.1126/science.1208163.

CALVO, E., PELEJERO, C. & LOGAN, G. A. 2003. Pressurized liquid extraction of selected molecular biomarkers in deep sea sediments used as proxies in paleoceanography. *Journal of Chromatography A,* 989, 197-205 doi:10.1016/S0021-9673(03)00119-5.

CHASE, Z., ANDERSON, R. F., FLEISHER, M. Q. & KUBIK, P. W. 2003. Accumulation of biogenic and lithogenic material in the Pacific sector of the Southern Ocean during the past 40,000 years. *Deep Sea Research Part II: Topical Studies in Oceanography,* 50, 799-832 doi:10.1016/S0967-0645(02)00595-7.

COSTA, K. M., HAYES, C. T., ANDERSON, R. F., PAVIA, F. J., BAUSCH, A., DENG, F., DUTAY, J.-C., GEIBERT, W., HEINZE, C., HENDERSON, G., HILLAIRE-MARCEL, C., HOFFMANN, S., JACCARD, S. L., JACOBEL, A. W., KIENAST, S. S., KIPP, L., LERNER, P., LIPPOLD, J., LUND, D., MARCANTONIO, F., MCGEE, D., MCMANUS, J. F., MEKIK, F., MIDDLETON, J. L., MISSIAEN, L., NOT, C., PICHAT, S., ROBINSON, L. F., ROWLAND, G. H., ROY-BARMAN, M., TAGLIABUE, A., TORFSTEIN, A., WINCKLER, G. & ZHOU, Y. 2020. 230Th Normalization: New Insights on an Essential Tool for Quantifying Sedimentary Fluxes in the Modern and Quaternary Ocean. *Paleoceanography and Paleoclimatology,* 35, e2019PA003820 doi:10.1029/2019pa003820.

DEVRIES, T. 2014. The oceanic anthropogenic CO2 sink: Storage, air-sea fluxes, and transports over the industrial era. *Global Biogeochemical Cycles,* 28, 631-647 doi:10.1002/2013gb004739.

ELDERFIELD, H. & GANSSEN, G. 2000. Past temperature and δ18O of surface ocean waters inferred from foraminiferal Mg/Ca ratios. *Nature,* 405, 442 doi:10.1038/35013033.

EZAT, M. M., RASMUSSEN, T. L., HONISCH, B., GROENEVELD, J. & DEMENOCAL, P. 2017. Episodic release of CO2 from the high-latitude North Atlantic Ocean during the last 135 kyr. *Nature Communications,* 8, 1-10 doi:10.1038/ncomms14498.

FOSTER, G. L. 2008. Seawater pH, PCO2 and CO32- variations in the Caribbean Sea over the last 130 kyr: A boron isotope and B/Ca study of planktic forminifera. *Earth and Planetary Science Letters,* 271, 254-266 doi:10.1016/j.epsl.2008.04.015.

FOSTER, G. L., HÖNISCH, B., PARIS, G., DWYER, G. S., RAE, J. W. B., ELLIOTT, T., GAILLARDET, J., HEMMING, N. G., LOUVAT, P. & VENGOSH, A. 2013. Interlaboratory comparison of boron isotope analyses of boric acid, seawater and marine CaCO3 by MC-ICPMS and NTIMS. *Chemical Geology,* 358, 1-14 doi:10.1016/j.chemgeo.2013.08.027.

FOSTER, G. L. & RAE, J. W. B. 2016. Reconstructing Ocean pH with Boron Isotopes in Foraminifera. *Annual Review of Earth and Planetary Sciences,* 44, 207-237 doi:10.1146/annurev-earth-060115-012226.

FOSTER, G. L. & SEXTON, P. F. 2014. Enhanced carbon dioxide outgassing from the eastern equatorial Atlantic during the last glacial. *Geology,* 42, 1003-1006 doi:10.1130/G35806.1.

FRANCOIS, R., FRANK, M., LOEFF, M. M. R. V. D. & BACON, M. P. 2004. 230Th normalization: An essential tool for interpreting sedimentary fluxes during the late Quaternary. *Paleoceanography,* 19 doi:10.1029/2003PA000939.

GALBRAITH, E. D. & JACCARD, S. L. 2015. Deglacial weakening of the oceanic soft tissue pump: global constraints from sedimentary nitrogen isotopes and oxygenation proxies. *Quaternary Science Reviews,* 109, 38-48 doi:10.1016/j.quascirev.2014.11.012.

GALBRAITH, E. D., JACCARD, S. L., PEDERSEN, T. F., SIGMAN, D. M., HAUG, G. H., COOK, M., SOUTHON, J. R. & FRANCOIS, R. 2007. Carbon dioxide release from the North Pacific abyss during the last deglaciation. *Nature,* 449, 890-893 doi:http://www.nature.com/nature/journal/v449/n7164/suppinfo/nature06227_S1.html.

GALBRAITH, E. D. & SKINNER, L. C. 2020. The Biological Pump During the Last Glacial Maximum. *Annual Review of Marine Science,* 12, 559-586 doi:10.1146/annurev-marine-010419-010906.

GOTTSCHALK, J., SKINNER, L. C., LIPPOLD, J., VOGEL, H., FRANK, N., JACCARD, S. L. & WAELBROECK, C. 2016. Biological and physical controls in the Southern Ocean on past millennial-scale atmospheric CO2 changes. *Nature Communications,* 7, 11539 doi:10.1038/ncomms11539.

GRAY, W. R., RAE, J. W. B., WILLS, R. C. J., SHEVENELL, A. E., TAYLOR, B., BURKE, A., FOSTER, G. L. & LEAR, C. H. 2018. Deglacial upwelling, productivity and CO2 outgassing in the North Pacific Ocean. *Nature Geoscience,* 11, 340-344 doi:10.1038/s41561-018-0108-6.

HAIN, M. P., FOSTER, G. L. & CHALK, T. 2018. Robust Constraints on Past CO2 Climate Forcing From the Boron Isotope Proxy. *Paleoceanography and Paleoclimatology,* 33, 1099-1115 doi:10.1029/2018pa003362.

HENEHAN, M. J., FOSTER, G. L., BOSTOCK, H. C., GREENOP, R., MARSHALL, B. J. & WILSON, P. A. 2016. A new boron isotope-pH calibration for Orbulina universa, with implications for understanding and accounting for ‘vital effects’. *Earth and Planetary Science Letters,* 454, 282-292 doi:10.1016/j.epsl.2016.09.024.

HENEHAN, M. J., FOSTER, G. L., RAE, J. W. B., PRENTICE, K. C., EREZ, J., BOSTOCK, H. C., MARSHALL, B. J. & WILSON, P. A. 2015. Evaluating the utility of B/Ca ratios in planktic foraminifera as a proxy for the carbonate system: A case study of Globigerinoides ruber. *Geochemistry, Geophysics, Geosystems,* 16, 1052-1069 doi:10.1002/2014gc005514.

HOGG, A. G., HUA, Q., BLACKWELL, P. G., NIU, M., BUCK, C. E., GUILDERSON, T. P., HEATON, T. J., PALMER, J. G., REIMER, P. J., REIMER, R. W., TURNEY, C. S. M. & ZIMMERMAN, S. R. H. 2016. SHCal13 Southern Hemisphere Calibration, 0–50,000 Years cal BP. *Radiocarbon,* 55, 1889-1903 doi:10.2458/azu_js_rc.55.16783.

JACCARD, S., HAYES, C. T., MARTÍNEZ-GARCÍA, A., HODELL, D., ANDERSON, R. F., SIGMAN, D. M. & HAUG, G. 2013. Two modes of change in Southern Ocean productivity over the past million years. *Science,* 339, 1419-1423 doi:10.1126/science.1227545.

JACCARD, S. L. & GALBRAITH, E. D. 2012. Large climate-driven changes of oceanic oxygen concentrations during the last deglaciation. *Nature Geoscience,* 5, 151-156 doi:10.1038/ngeo1352.

JACCARD, S. L., GALBRAITH, E. D., MARTÍNEZ-GARCÍA, A. & ANDERSON, R. F. 2016. Covariation of deep Southern Ocean oxygenation and atmospheric CO2 through the last ice age. *Nature,* 530, 207-210 doi:10.1038/nature16514.

KISS, E. 1988. Ion-exchange separation and spectrophotometric determination of boron in geological materials. *Analytica Chimica Acta,* 211, 243-256 doi:10.1016/S0003-2670(00)83684-3.

KÖHLER, P., JOOS, F., GERBER, S. & KNUTTI, R. 2005. Simulated changes in vegetation distribution, land carbon storage, and atmospheric CO2 in response to a collapse of the North Atlantic thermohaline circulation. *Climate Dynamics,* 25, 689 doi:10.1007/s00382-005-0058-8.

KORNILOVA, O. & ROSELL-MELÉ, A. 2003. Application of microwave-assisted extraction to the analysis of biomarker climate proxies in marine sediments. *Organic Geochemistry,* 34, 1517-1523 doi:10.1016/S0146-6380(03)00155-4.

KUBOTA, K., YOKOYAMA, Y., ISHIKAWA, T., SAGAWA, T., IKEHARA, M. & YAMAZAKI, T. 2019. Equatorial Pacific seawater pCO2 variability since the last glacial period. *Scientific Reports,* 9, 13814 doi:10.1038/s41598-019-49739-0.

LAMBERT, F., BIGLER, M., STEFFENSEN, J. P., HUTTERLI, M. & FISCHER, H. 2012. Centennial mineral dust variability in high-resolution ice core data from Dome C, Antarctica. *Clim. Past,* 8, 609-623 doi:10.5194/cp-8-609-2012.

LAMY, F., GERSONDE, R., WINCKLER, G., ESPER, O., JAESCHKE, A., KUHN, G., ULLERMANN, J., MARTÍNEZ-GARCIA, A., LAMBERT, F. & KILIAN, R. 2014. Increased dust deposition in the Pacific Southern Ocean during glacial periods. *Science,* 343, 403-407 doi:10.1126/science.1245424.

LEMARCHAND, D., GAILLARDET, J., GÖPEL, C. & MANHÈS, G. 2002. An optimized procedure for boron separation and mass spectrometry analysis for river samples. *Chemical Geology,* 182, 323-334 doi:10.1016/S0009-2541(01)00329-1.

LOUGHEED, B. C. & OBROCHTA, S. P. 2019. A Rapid, Deterministic Age-Depth Modeling Routine for Geological Sequences With Inherent Depth Uncertainty. *Paleoceanography and Paleoclimatology,* 34, 122-133 doi:10.1029/2018pa003457.

MARTINEZ-BOTI, M. A., MARINO, G., FOSTER, G. L., ZIVERI, P., HENEHAN, M. J., RAE, J. W. B., MORTYN, P. G. & VANCE, D. 2015. Boron isotope evidence for oceanic carbon dioxide leakage during the last deglaciation. *Nature,* 518, 219-222 doi:10.1038/nature14155.

MARTÍNEZ-BOTÍ, M. A., MARINO, G., FOSTER, G. L., ZIVERI, P., HENEHAN, M. J., RAE, J. W. B., MORTYN, P. G. & VANCE, D. 2015. Boron isotope evidence for oceanic carbon dioxide leakage during the last deglaciation. *Nature,* 518, 219-222 doi:10.1038/nature14155.

MARTÍNEZ-GARCÍA, A., SIGMAN, D. M., REN, H., ANDERSON, R. F., STRAUB, M., HODELL, D. A., JACCARD, S. L., EGLINTON, T. I. & HAUG, G. H. 2014. Iron Fertilization of the Subantarctic Ocean During the Last Ice Age. *Science,* 343, 1347-1350 doi:10.1126/science.1246848.

MAXSON, C. R., BOSTOCK, H. C., MACKINTOSH, A., MIKALOFF-FLETCHER, S., MCCAVE, N. & NEIL, H. L. 2019. Modern, Preindustrial, and Past (Last 25 ka) Carbon Isotopic (δ13C) Variability in the Surface Waters of the Southwest Pacific. *Paleoceanography and Paleoclimatology,* 34, 692-714 doi:10.1029/2018PA003441.

MOY, A. D., PALMER, M. R., HOWARD, W. R., BIJMA, J., COOPER, M. J., CALVO, E., PELEJERO, C., GAGAN, M. K. & CHALK, T. B. 2019. Varied contribution of the Southern Ocean to deglacial atmospheric CO2 rise. *Nature Geoscience,* 12, 1006-1011 doi:10.1038/s41561-019-0473-9.

NAIK, S. S., DIVAKAR NAIDU, P., FOSTER, G. L. & MARTÍNEZ-BOTÍ, M. A. 2015. Tracing the strength of the southwest monsoon using boron isotopes in the eastern Arabian Sea. *Geophysical Research Letters,* 42, 1450-1458 doi:10.1002/2015GL063089.

NINNEMANN, U. S. & CHARLES, C. D. 1997. Regional differences in Quaternary subantarctic nutrient cycling: Link to intermediate and deep water ventilation. *Paleoceanography,* 12**,** 560-567 doi:10.1029/97pa01032.

PALMER, M. R. & PEARSON, P. N. 2003. A 23,000-Year Record of Surface Water pH and pCO2 in the Western Equatorial Pacific Ocean. *Science,* 300**,** 480-482 doi:10.1126/science.1080796.

RAE, J. W. B., BURKE, A., ROBINSON, L. F., ADKINS, J. F., CHEN, T., COLE, C., GREENOP, R., LI, T., LITTLEY, E. F. M., NITA, D. C., STEWART, J. A. & TAYLOR, B. J. 2018. CO2 storage and release in the deep Southern Ocean on millennial to centennial timescales. *Nature,* 562**,** 569-573 doi:10.1038/s41586-018-0614-0.

RAE, J. W. B., FOSTER, G. L., SCHMIDT, D. N. & ELLIOTT, T. 2011. Boron isotopes and B/Ca in benthic foraminifera: Proxies for the deep ocean carbonate system. *Earth and Planetary Science Letters,* 302**,** 403-413 doi:10.1016/j.epsl.2010.12.034.

RAITZSCH, M., BIJMA, J., BENTHIEN, A., RICHTER, K.-U., STEINHOEFEL, G. & KUČERA, M. 2018. Boron isotope-based seasonal paleo-pH reconstruction for the Southeast Atlantic – A multispecies approach using habitat preference of planktonic foraminifera. *Earth and Planetary Science Letters,* 487**,** 138-150 doi:10.1016/j.epsl.2018.02.002.

ROBERTS, J., GOTTSCHALK, J., SKINNER, L. C., PECK, V. L., KENDER, S., ELDERFIELD, H., WAELBROECK, C., VÁZQUEZ RIVEIROS, N. & HODELL, D. A. 2016. Evolution of South Atlantic density and chemical stratification across the last deglaciation. *Proceedings of the National Academy of Sciences,* 113**,** 514-519 doi:10.1073/pnas.1511252113.

SARMIENTO, J. L., GRUBER, N., BRZEZINSKI, M. A. & DUNNE, J. P. 2004. High-latitude controls of thermocline nutrients and low latitude biological productivity. *Nature,* 427**,** 56 doi:10.1038/nature02127.

SCHMITT, J., SCHNEIDER, R., ELSIG, J., LEUENBERGER, D., LOURANTOU, A., CHAPPELLAZ, J., KÖHLER, P., JOOS, F., STOCKER, T. F., LEUENBERGER, M. & FISCHER, H. 2012. Carbon Isotope Constraints on the Deglacial CO2 Rise from Ice Cores. *Science,* 336**,** 711-714 doi:10.1126/science.1217161.

SHAO, J., STOTT, L. D., GRAY, W. R., GREENOP, R., PECHER, I., NEIL, H. L., COFFIN, R. B., DAVY, B. & RAE, J. W. B. 2019. Atmosphere-Ocean CO2 Exchange Across the Last Deglaciation from the Boron Isotope Proxy. *Paleoceanography and Paleoclimatology,* 34**,** 1650-1670 doi:10.1029/2018pa003498.

SIGMAN, D. M., HAIN, M. P. & HAUG, G. H. 2010. The polar ocean and glacial cycles in atmospheric CO2 concentration. *Nature,* 466**,** 47-55 doi:10.1038/nature09149.

SKINNER, L., MCCAVE, I. N., CARTER, L., FALLON, S., SCRIVNER, A. E. & PRIMEAU, F. 2015. Reduced ventilation and enhanced magnitude of the deep Pacific carbon pool during the last glacial period. *Earth and Planetary Science Letters,* 411**,** 45-52 doi:https://doi.org/10.1016/j.epsl.2014.11.024.

SKINNER, L. C., FALLON, S., WAELBROECK, C., MICHEL, E. & BARKER, S. 2010. Ventilation of the Deep Southern Ocean and Deglacial CO2 Rise. *Science,* 328**,** 1147-1151 doi:10.1126/science.1183627.

SKINNER, L. C., WAELBROECK, C., SCRIVNER, A. E. & FALLON, S. J. 2014. Radiocarbon evidence for alternating northern and southern sources of ventilation of the deep Atlantic carbon pool during the last deglaciation. *Proceedings of the National Academy of Sciences,* 111**,** 5480-5484 doi:10.1073/pnas.1400668111.

SPERO, H. J. & LEA, D. W. 2002. The Cause of Carbon Isotope Minimum Events on Glacial Terminations. *Science,* 296**,** 522-525 doi:10.1126/science.1069401.

STEWART, J. A., CHRISTOPHER, S. J., KUCKLICK, J. R., BORDIER, L., CHALK, T. B., DAPOIGNY, A., DOUVILLE, E., FOSTER, G. L., GRAY, W. R., GREENOP, R., GUTJAHR, M., HEMSING, F., HENEHAN, M. J., HOLDSHIP, P., HSIEH, Y.-T., KOLEVICA, A., LIN, Y.-P., MAWBEY, E. M., RAE, J. W. B., ROBINSON, L. F., SHUTTLEWORTH, R., YOU, C.-F., ZHANG, S. & DAY, R. D. NIST RM 8301 Boron Isotopes in Marine Carbonate (Simulated Coral and Foraminifera Solutions):

Inter-laboratory δ11B and Trace Element Ratio Value Assignment. *Geostandards and Geoanalytical Research,* n/a doi:10.1111/ggr.12363.

STUDER, A. S., SIGMAN, D. M., MARTÍNEZ-GARCÍA, A., BENZ, V., WINCKLER, G., KUHN, G., ESPER, O., LAMY, F., JACCARD, S. L., WACKER, L., OLEYNIK, S., GERSONDE, R. & HAUG, G. H. 2015. Antarctic Zone nutrient conditions during the last two glacial cycles. *Paleoceanography,* 30**,** 845-862 doi:10.1002/2014pa002745.

TAKAHASHI, T., SUTHERLAND, S. C., WANNINKHOF, R., SWEENEY, C., FEELY, R. A., CHIPMAN, D. W., HALES, B., FRIEDERICH, G., CHAVEZ, F., SABINE, C., WATSON, A., BAKKER, D. C. E., SCHUSTER, U., METZL, N., YOSHIKAWA-INOUE, H., ISHII, M., MIDORIKAWA, T., NOJIRI, Y., KÖRTZINGER, A., STEINHOFF, T., HOPPEMA, M., OLAFSSON, J., ARNARSON, T. S., TILBROOK, B., JOHANNESSEN, T., OLSEN, A., BELLERBY, R., WONG, C. S., DELILLE, B., BATES, N. R. & DE BAAR, H. J. W. 2009. Climatological mean and decadal change in surface ocean pCO2, and net sea–air CO2 flux over the global oceans. *Deep Sea Research Part II: Topical Studies in Oceanography,* 56**,** 554-577 doi:10.1016/j.dsr2.2008.12.009.

TAKAHASHI, T., SWEENEY, C., HALES, B., CHIPMAN, D., NEWBERGER, T., GODDARD, J., IANNUZZI, R. & SUTHERLAND, S. 2012. The Changing Carbon Cycle in the Southern Ocean. *Oceanography,* 25**,** 26-37 doi:10.5670/oceanog.2012.71.

THÖLE, L. M., AMSLER, H. E., MORETTI, S., AUDERSET, A., GILGANNON, J., LIPPOLD, J., VOGEL, H., CROSTA, X., MAZAUD, A., MICHEL, E., MARTÍNEZ-GARCÍA, A. & JACCARD, S. L. 2019. Glacial-interglacial dust and export production records from the Southern Indian Ocean. *Earth and Planetary Science Letters,* 525**,** 115716 doi:10.1016/j.epsl.2019.115716.

TOGGWEILER, J. R. 1999. Variation of atmospheric CO2 by ventilation of the ocean's deepest water. *Paleoceanography,* 14**,** 571-588 doi:10.1029/1999PA900033.

TOGGWEILER, J. R., DRUFFEL, E. R. M., KEY, R. M. & GALBRAITH, E. D. 2019. Upwelling in the Ocean Basins North of the ACC: 2. How Cool Subantarctic Water Reaches the Surface in the Tropics. *Journal of Geophysical Research: Oceans,* 124**,** 2609-2625 doi:10.1029/2018jc014795.

TRUDGILL, M., SHUTTLEWORTH, R., BOSTOCK, H. C., BURKE, A., COOPER, M. J., GREENOP, R. & FOSTER, G. L. Submitted. The Flux and Provenance of Dust Delivered to the SW Pacific During the Last Glacial Maximum. *Paleoceanography and Paleoclimatology*.

VENZ, K. A. & HODELL, D. A. 2002. New evidence for changes in Plio–Pleistocene deep water circulation from Southern Ocean ODP Leg 177 Site 1090. *Palaeogeography, Palaeoclimatology, Palaeoecology,* 182**,** 197-220 doi:10.1016/S0031-0182(01)00496-5.

VERES, D., BAZIN, L., LANDAIS, A., TOYÉ MAHAMADOU KELE, H., LEMIEUX-DUDON, B., PARRENIN, F., MARTINERIE, P., BLAYO, E., BLUNIER, T., CAPRON, E., CHAPPELLAZ, J., RASMUSSEN, S. O., SEVERI, M., SVENSSON, A., VINTHER, B. & WOLFF, E. W. 2013. The Antarctic ice core chronology (AICC2012): an optimized multi-parameter and multi-site dating approach for the last 120 thousand years. *Clim. Past,* 9**,** 1733-1748 doi:10.5194/cp-9-1733-2013.

VILLANUEVA, J., PELEJERO, C. & GRIMALT, J. O. 1997. Clean-up procedures for the unbiased estimation of C37 alkenone sea surface temperatures and terrigenous n-alkane inputs in paleoceanography. *Journal of Chromatography A,* 757**,** 145-151 doi:10.1016/S0021-9673(96)00669-3.

WANG, X. T., SIGMAN, D. M., PROKOPENKO, M. G., ADKINS, J. F., ROBINSON, L. F., HINES, S. K., CHAI, J., STUDER, A. S., MARTÍNEZ-GARCÍA, A., CHEN, T. & HAUG, G. H. 2017. Deep-sea coral evidence for lower Southern Ocean surface nitrate concentrations during the last ice age. *Proceedings of the National Academy of Sciences,* 114**,** 3352-3357 doi:10.1073/pnas.1615718114.

ZIEGLER, M., DIZ, P., HALL, I. R. & ZAHN, R. 2013. Millennial-scale changes in atmospheric CO2 levels linked to the Southern Ocean carbon isotope gradient and dust flux. *Nature Geoscience,* 6**,** 457-461 doi:10.1038/ngeo1782.